Endocrine-Exocrine Signaling Drives Obesity-Associated Pancreatic Ductal Adenocarcinoma

As Published: 10.1016/J.CELL.2020.03.062

Publisher: Elsevier BV

Persistent URL: https://hdl.handle.net/1721.1/134176

Version: Author's final manuscript: final author's manuscript post peer review, without publisher's formatting or copy editing

HHS Public Access

Author manuscript

Cell. Author manuscript; available in PMC 2021 May 14.

Published in final edited form as:

Cell. 2020 May 14; 181(4): 832–847.e18. doi:10.1016/j.cell.2020.03.062.

Endocrine-exocrine signaling drives obesity-associated pancreatic ductal adenocarcinoma

Katherine Minjee Chung[1,19], **Jaffarguriqbal Singh**[2,3,19], **Lauren Lawres**[2,3,19], **Kimberly Judith Dorans**[1,19], **Cathy Garcia**[2,3], **Daniel B. Burkhardt**[2], **Rebecca Robbins**[1], **Arjun Bhutkar**[1], **Rebecca Cardone**[4], **Xiaojian Zhao**[4], **Ana Babic**[5], **Sara A. Vayrynen**[5], **Andressa Dias Costa**[5], **Jonathan A. Nowak**[6], **Daniel T. Chang**[7], **Richard F. Dunne**[8], **Aram F. Hezel**[8], **Albert C. Koong**[9], **Joshua J. Wilhelm**[10], **Melena D. Bellin**[10,11], **Vibe Nylander**[12], **Anna L. Gloyn**[12,13,14,18], **Mark I. McCarthy**[12,13,14,17], **Richard G. Kibbey**[4], **Smita Krishnaswamy**[2], **Brian M. Wolpin**[5], **Tyler Jacks**[1,15], **Charles S. Fuchs**[16], **Mandar Deepak Muzumdar**[2,3,16,20]

[1]Koch Institute for Integrative Cancer Research at MIT, Cambridge, MA 02139, USA

[2]Department of Genetics, Yale University School of Medicine, New Haven, CT 06510, USA

[3]Yale Cancer Biology Institute, Yale University, West Haven, CT 06516, USA

[4]Departments of Internal Medicine and Cellular & Molecular Physiology, Yale University School of Medicine, New Haven, CT 06520, USA

[5]Department of Medical Oncology, Dana-Farber Cancer Institute, Harvard Medical School, Boston, MA, 02114, USA

Correspondence: mandar.muzumdar@yale.edu.

AUTHOR CONTRIBUTIONS

T.J., C.S.F., and M.D.M. designed and supervised the study; K.M.C., J.S., L.L., K.J.D., C.G., R.R., and M.D.M. performed experiments; D.B.B and S.K. conducted scRNA-seq computational analyses; A.B. conducted exome computational analyses and bulk RNA-seq expression signature analyses; R.C., X.Z., and R.G.K. performed and analyzed islet isolation and perifusion studies; A.B., J.N., S.A.V., A.D.C., and B.M.W. performed targeted exome and IHC analyses on human PDAC; D.T.C., R.F.D., A.F.H., A.C.K., J.J.W., and M.D.B. provided human PDAC and pancreatitis biospecimens; V.N., A.L.G., and M.I.M. acquired and analyzed human donor islet gene expression data; M.D.M. wrote the manuscript with comments from all authors.

DECLARATION OF INTERESTS

K.J.D. is currently an employee of Sherlock Biosciences. M.D.B. acknowledges research support from ViaCyte and Dexcom and serves on the medical advisory boards for Novo Nordisk and ARIEL Precision Medicine. A.L.G. has received honoraria from Merck and Novo Nordisk and has received research funding from Novo Nordisk. M.I.M. has served on advisory panels for Pfizer, Novo Nordisk, Zoe Global; he has received honoraria from Merck, Pfizer, Novo Nordisk and Eli Lilly and research funding from Abbvie, Astra Zeneca, Boehringer Ingelheim, Eli Lilly, Janssen, Merck, Novo Nordisk, Pfizer, Roche, Sanofi Aventis, Servier, and Takeda. As of June 2019, M.I.M. is an employee of Genentech, and a holder of Roche stock. R.G.K. is co-founder and a Scientific Advisory Board member of Elucidata, a Consultant/Advisory Board member for Agios, Janssen, BI-Lilly, and Pfizer, and a recipient of sponsored research agreements from Agios, AstraZeneca/BMS, Lilly, Pfizer, and Poxel. S.K. is a paid scientific advisor to AI Therapeutics. B.M.W. declares research funding from Celgene Inc. and Eli Lilly & Company, and consulting for BioLineRx Ltd., Celgene Inc., G1 Therapeutics Inc., and GRAIL Inc. T.J. is a Board of Directors member of Amgen and Thermo Fisher Scientific, co-Founder and Scientific Advisory Board member of Dragonfly Therapeutics, co-founder of T2 Biosystems, and Scientific Advisory Board member of SQZ Biotech with equity holding in all five companies; he receives funding from the Johnson & Johnson Lung Cancer Initiative and Calico. C.S.F. reports receiving personal fees from Eli Lilly, Entrinsic Health, Pfizer, Merck, Sanofi, Roche, Genentech, Merrimack Pharma, Dicerna, Bayer, Celgene, Agios, Gilead Sciences, Five Prime Therapeutics, Taiho, KEW, and CytomX Therapeutics and receiving support from CytomX Therapeutics. M.D.M. acknowledges research support from Genentech.

[6]Department of Pathology, Brigham and Women's Hospital, Harvard Medical School, Boston, MA 02115, USA

[7]Department of Radiation Oncology, Stanford Cancer Institute, Stanford, CA 94305, USA

[8]Division of Hematology and Oncology, Department of Medicine, Wilmot Cancer Institute, University of Rochester Medical Center, Rochester, NY 14627, USA

[9]Department of Radiation Oncology, The University of Texas MD Anderson Cancer Center, Houston, TX 77030, USA

[10]Schulze Diabetes Institute and Department of Surgery, University of Minnesota Medical Center, Minneapolis, MN 55454, USA

[11]Department of Pediatrics, University of Minnesota Medical Center, Minneapolis, MN 55454

[12]Wellcome Centre for Human Genetics, Nuffield Department of Medicine, University of Oxford, Oxford, OX3 7BN, UK

[13]Oxford Centre for Diabetes, Endocrinology and Metabolism, Radcliffe Department of Medicine, University of Oxford, Oxford, OX3 7LE, UK

[14]Oxford NIHR Biomedical Research Centre, Oxford University Hospitals Trust, Oxford, OX3 7LE, UK

[15]Howard Hughes Medical Institute, Massachusetts Institute of Technology, Cambridge, MA 02139, USA

[16]Yale Cancer Center, Smilow Cancer Hospital, New Haven, CT 06511, USA

[17]Current address: Genentech, 340 Point San Bruno Boulevard, South San Francisco, CA 94080, USA

[18]Current address: Department of Pediatrics, Stanford School of Medicine, Stanford, CA 94305, USA

[19]These authors contributed equally

[20]Corresponding Author/Lead Contact

SUMMARY

Obesity is a major modifiable risk factor for pancreatic ductal adenocarcinoma (PDAC), yet how and when obesity contributes to PDAC progression is not well understood. Leveraging an autochthonous mouse model, we demonstrate a causal and reversible role for obesity in early PDAC progression, showing that obesity markedly enhances tumorigenesis, while genetic or dietary induction of weight loss intercepts cancer development. Molecular analyses of human and murine samples define microenvironmental consequences of obesity that foster tumorigenesis rather than new driver gene mutations, including significant pancreatic islet cell adaptation in obesity-associated tumors. Specifically, we identify aberrant beta cell expression of the peptide hormone cholecystokinin (Cck) in response to obesity and show that islet Cck promotes oncogenic *Kras*-driven pancreatic ductal tumorigenesis. Our studies argue that PDAC progression is driven by local obesity-associated changes in the tumor microenvironment and implicate endocrine-exocrine signaling beyond insulin in PDAC development.

Graphical Abstract

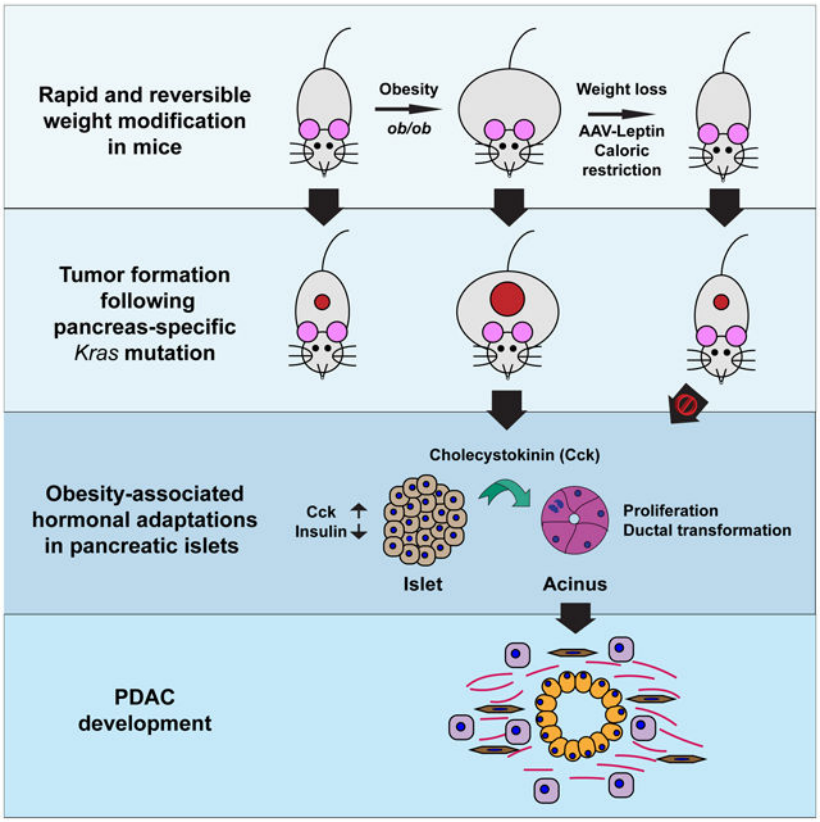

In Brief

Obesity is an intrinsic driver of PDAC in mice, leading to a remodeling of beta cells to increase CCK secretion, and playing a role early in pancreatic cancer development that can be intercepted by weight loss.

Keywords

Pancreatic cancer; obesity; cholecystokinin; pancreatic islets; beta cells; tumor microenvironment; genetically engineered mouse models; leptin

INTRODUCTION

Pancreatic ductal adenocarcinoma (PDAC) is the third leading cause of cancer death in the United States and is expected to become the second within the next few years (Rahib et al., 2014; Siegel et al., 2020). Despite the development of combination chemotherapy, targeted small molecules, and immunotherapies that have revolutionized cancer care, long-term survival in PDAC remains low at ~10% (Ryan et al., 2014; Siegel et al., 2020). In search of drug targets, genomic studies have identified frequent mutations in the proto-oncogene *KRAS*, occurring in >90% of human PDAC tumors (Bailey et al., 2016; TCGA Research Network, 2017). Unfortunately, no effective direct KRAS inhibitors are currently approved

for clinical use (Papke and Der, 2017). Moreover, our recent work demonstrated that PDAC cells can survive genetic ablation of *KRAS* both *in vitro* and *in vivo* (Chen et al., 2018; Muzumdar et al., 2017), arguing that resistance will subvert even the very best KRAS inhibitors. Therefore, alternative paradigms beyond genetic factors need to be explored to develop novel therapeutic and preventative strategies for PDAC.

Epidemiologic studies in prospective human cohorts have shown that body-mass index (BMI), a surrogate measure of obesity, is associated with increased PDAC risk, more advanced disease at diagnosis, and worse survival (Larsson et al., 2007; Yuan et al., 2013). Yet, how obesity contributes to PDAC development remains poorly understood. Previous research showed that high-fat diet (HFD)-induced obesity promotes tumor progression in transplant and autochthonous models of PDAC (Incio et al., 2016; Khasawneh et al., 2009; Philip et al., 2013; Chang et al., 2017; Zaytouni et al., 2017; Zyromski et al., 2009), and implicated dysregulation of fatty acid and nitrogen metabolism (Khasawneh et al., 2009; Zaytouni et al., 2017), COX2 activation (Philip et al., 2013), and aberrations in the desmoplastic response (Incio et al., 2016; Khasawneh et al., 2009; Chang et al., 2017) as potential mechanisms. These studies were limited by slow obesity onset in HFD models, as well as variations in fat content, types of fat, and age of administration in HFD protocols, all of which can confound results (Speakman, 2019). Importantly, these approaches provided no information on whether – and at what point – weight loss or other anti-obesity interventions might influence PDAC progression, despite significant clinical implications (Massetti et al., 2017).

To overcome these important limitations, we developed a rapid and reversible autochthonous model of obesity-associated PDAC. We demonstrate that obesity plays a causal – and reversible – role in early PDAC progression. We further identify aberrant expression of the hormone cholecystokinin (Cck) in islet beta cells in tumors as an adaptive response to obesity and show that islet Cck overexpression itself promotes pancreatic ductal tumorigenesis. Together, these studies link obesity, changes in the local microenvironment, and tumorigenesis through a previously unappreciated endocrine-exocrine signaling axis in PDAC development.

RESULTS

Obesity drives pancreatic tumorigenesis in mice

To model obesity-associated pancreatic cancer, we crossed leptin-deficient (*ob/ob*) mice with *KC (Pdx1-Cre; Kras*$^{LSL\text{-}G12D/WT}$) mice predisposed to the development of precursor pancreatic intraepithelial neoplasia (PanINs) (Hingorani et al., 2003) to yield *KC; ob/ob (KCO*) mice (Figure 1A). Unlike HFD models, *ob/ob* mice exhibit early onset obesity due to impaired appetite suppression and decreased metabolism (Friedman, 2019). *KCO* mice were obese and developed increased primary ductal tumor burden (Figures 1B-D). They also showed enhanced progression to adenocarcinoma and markedly shortened survival compared to non-obese *KC* mice (Figures 1E-F). We similarly observed decreased survival using a distinct obesity model due to leptin receptor mutation (*db/db*) (Figures S1A-B). These phenotypes were significantly more severe than seen in HFD models (Khasawneh et al., 2009; Philip et al., 2013; Chang et al., 2017), corresponding to the degree of obesity.

Consistent with human epidemiologic studies that demonstrate an association between obesity and pancreatic cancer, but not lung cancer (Lauby-Secretan et al., 2016), obesity induced by neither HFD nor *ob/ob* genotype shortened survival in lung cancer initiated by oncogenic *Kras* (Figures S1C-F). Thus, these results support a specific effect of obesity on *Kras*-driven PDAC progression.

Weight loss intercepts early tumor progression in *KCO* mice

We chose the *ob/ob* model because it affords rapid reversal of the obesity phenotype through leptin restoration to study the effects of weight loss on PDAC development. We generated an adeno-associated viruses (AAV) that directs sustained leptin secretion (AAV-Leptin) following a single intramuscular injection (Figures 2A and S2A-B). AAV-Leptin reversed multiple phenotypes of leptin deficiency including obesity, hyperglycemia, and infertility (Figures 2B and S2C-D), as seen with leptin protein replacement (Friedman, 2019). Remarkably, early AAV-Leptin administration impeded tumor progression proportional to the degree of weight loss (Figures 2C-D). In contrast, late AAV-Leptin administration (following advanced tumor development) induced weight loss without impacting survival (Figures S2E-F). Moreover, leptin induced on-target downstream signaling in advanced murine PDAC cells *in vitro* but did not alter cell viability (Figures S2G-H). These data support a stage-specific effect of obesity on early PDAC development. Experiments with caloric restriction argue that it is weight loss itself that impacts tumor progression – rather than leptin signaling. Young *KCO* mice subject to caloric restriction exhibited significantly reduced tumor burden compared to mice fed ad libitum (Figures 2E-F), demonstrating the potential to halt or delay obesity-driven PDAC progression with weight loss.

Obesity promotes PDAC progression independent of new mutations

We next sought to identify the mechanisms by which obesity contributes to pancreatic tumorigenesis in this model. We postulated that obesity might induce DNA damage in the setting of enhanced oxidative stress (Usman and Volpi, 2018) and that tumor progression in *KCO* mice would depend on additional driver gene mutations beyond oncogenic *Kras*. Precedent for this hypothesis is provided by acceleration of oncogenic *Kras*-induced pancreatic tumor development in mice with inactivating mutations in *Trp53, Cdkn2a*, or *Smad4* (Bardeesy et al., 2006a; Bardeesy et al., 2006b; Hingorani et al., 2005; Muzumdar et al., 2016) – the hallmark recurrently mutated tumor suppressor genes in human PDAC (Bailey et al., 2016; TCGA Research Network, 2017)). In further support, survival of *KCO* mice was comparable to what we previously observed (Muzumdar et al., 2016) in *KPC* mice (*Pdx1-Cre; Kras*$^{LSL\text{-}G12D/WT}$; *p53*$^{flox/WT}$or *Pdx1-Cre; Kras*$^{LSL\text{-}G12D/WT}$; *p53*$^{LSL\text{-}R172H/WT}$) harboring heterozygous mutations in*p53* (p=0.93, log-rank test). Surprisingly, however, immunohistochemistry (IHC) revealed persistent tumor suppressor protein expression, and exome sequencing confirmed the absence of inactivating point mutations in the associated genes (Figure 3 and Table S1). Furthermore, we did not observe recurrent pathogenic mutations in other known PDAC (Bailey et al., 2016; TCGA Research Network, 2017) or pan-cancer driver genes (Bailey et al., 2018) in *KCO* tumors (Tables S2-S3). Contrary to our expectations, these data argue that additional driver gene mutations are not required for obesity to promote pancreatic cancer development. To determine if a similar phenomenon is evident in human tumors, we performed targeted exome sequencing and IHC to evaluate

alterations of *KRAS, TP53, CDKN2A/p16,* and *SMAD4* in 184 human PDAC with known patient BMI at diagnosis (Table S4). Although we observed a significant increase in *SMAD4* loss with elevated BMI, the total number of driver gene alterations per tumor, which we have previously shown predicts worse outcomes in patients with localized PDAC (Qian et al., 2018), did not significantly differ across categories of BMI (Table S5). Together, these data suggest that obesity may promote pancreatic tumorigenesis independent of new driver mutations.

Tumors in obese mice show evidence of increased inflammation and fibrosis

To elucidate potential non-mutational mechanisms of PDAC progression, we performed bulk RNA sequencing (RNA-seq) on pancreata from obese *KCO* and non-obese *KC* and *KPC* mice exhibiting comparable tumor burden (Table S6). Using Independent Component Analysis (ICA), an unsupervised blind source separation technique (Hyvarinen and Oja, 2000; Muzumdar et al., 2017), we identified gene expression signatures associated with inflammation and fibrosis as upregulated in *KCO* compared to *KC/KPC* mice (Figures 4A-D and Tables S6), likely representing obesity-associated alterations in the tumor microenvironment. We confirmed abundant extracellular matrix deposition and immune cell infiltration by histologic analyses of *KCO* tumors (Figure 4E). To determine human relevance, we ranked primary human PDAC tumors from The Cancer Genome Atlas (TCGA) (TCGA Research Network, 2017) based on gene expression correlation to these *KCO* signatures. We classified tumors using previously-defined molecular subtypes (Bailey et al., 2016) and found the *KCO*-correlated tumors to be significantly enriched with the immunogenic subtype (Figure 4F), which is similarly associated with immune cell infiltration (Bailey et al., 2016; TCGA Research Network, 2017). These data revealed that alterations in the fibroinflammatory microenvironment are a major feature of obesity-associated pancreatic tumors and are consistent with prior work using HFD models (Incio et al., 2016; Chang et al., 2017).

Consequently, we tested the effects of anti-inflammatory (aspirin) and anti-fibrotic (metformin) (Chen et al., 2017; Rangarajan et al., 2018) drugs on tumor progression in *KCO* mice. We chose these specific agents because they have been shown to mitigate pancreatic cancer risk in selected (Li et al., 2009; Zhang et al., 2015), but not all (Khalaf et al., 2018), patient cohorts and are in widespread clinical use for other indications. Remarkably, neither aspirin nor metformin impacted tumor progression, immune cell infiltration, or fibrosis in *KCO* mice (Figure S3), indicating that these agents may have a limited role in preventing obesity-driven PDAC. Furthermore, these data left open the possibility that the obesity-associated changes in the fibroinflammatory microenvironment could be a consequence rather than a cause of pancreatic tumorigenesis. Therefore, we sought alternative mechanisms that may contribute to PDAC development in obesity.

Tumors in obese mice exhibit marked pancreatic islet adaptation

One of the most notable RNA-seq results was upregulation of genes associated with pancreatic islet cell function in *KCO* compared to *KC/KPC* pancreata (Figures 5A). Although expression levels of general neuroendocrine markers were mostly unchanged in *KCO* pancreata (Figure 5B), we observed a marked increase in the expression of genes

encoding islet prohormones, proteases that process them, and secretory granule proteins (Figure 5C). We confirmed gene expression data by IHC on islets in tumor-bearing mice. While glucagon (Gcg) and its proteolytic product GLP-1 are typically expressed in peripherally-located alpha cells in non-obese rodents (Barreto et al., 2010), *KCO* mice displayed an expansion of Gcg and GLP-1 production throughout islets (Figure 5D). These observations are consistent with prior research demonstrating increased GLP-1 secretion from islets of obese humans and mice (Linnemann et al., 2015). Together, our results support islet adaptation to enhance hormone production, processing, and secretion in the setting of obesity.

Given these findings, we postulated that enhanced local insulin secretion may promote pancreatic tumorigenesis in obese mice. Although *ob/ob* mice exhibited systemic hyperinsulinemia (Figure S4A), glucose-stimulated insulin secretion by primary islets derived from *ob/ob* mice was reduced (Figures S4B-D), consistent with severely impaired local insulin secretion. Furthermore, analysis of insulin receptor phosphorylation suggested comparable signaling activation in tumor cells from both *KC* and *KCO* mice (Figure S4E). These data argue against local increases in insulin or insulin signaling as a primary driver of pancreatic tumorigenesis. We tested this hypothesis further by treating *KCO* mice with the sodium-glucose co-transporter type 2 (SGLT2) inhibitor dapagliflozin, which blocks kidney reabsorption of glucose and attenuates obesity-associated hyperglycemia. *Slc5a2* (SGLT2) knockout in *db/db* mice improves islet function and maintenance by reducing beta cell glucotoxicity (Jurczak et al., 2011; Jurczak et al., 2018). Similarly, treatment with dapagliflozin reduced serum glucose and maintained higher circulating insulin and proinsulin (C-peptide) levels in *KCO* mice (Figures S4F-G), indicating preserved beta cell function. The variable effect of dapagliflozin on the maintenance of insulin production across *KCO* mice (Figure S4G) allowed us to quantitatively compare the relationship between insulin and tumor development in this model. We anticipated that if insulin was a main driver of tumorigenesis, tumor burden would be enhanced proportional to insulin production. Contrary to this hypothesis, C-peptide levels inversely correlated with tumor burden (Figure S4H), suggesting that alternative changes in islet hormone expression may play a greater role in tumor development.

Single cell RNA-sequencing identifies beta cell expression of *Cck* in obesity

To decipher islet hormone expression at higher resolution, we performed single-cell RNA sequencing (scRNA-seq) on islets isolated from congenic C57/B6 wild-type and *ob/ob* mice. Visualization using PHATE (Moon et al., 2019), a method for dimensionality reduction of single-cell data, displayed clusters corresponding to single hormone-expressing beta (insulin), alpha (glucagon), delta (somatostatin), and PP (Ppy) cells (Figure 6A). To characterize the differences between cells captured from *ob/ob* and wild-type islets, we used the newly developed MELD package (Burkhardt et al., 2019), which derives a likelihood score, called the Enhanced Experimental Signal (EES), for each cell to annotate regions of the cellular manifold that are enriched in the *ob/ob* or wild-type genotype. Examining the distribution of EES values within islet cell types, we observed only moderate overlap in beta cell populations from *ob/ob* and wild-type mice (Figure 6B), consistent with significant changes in gene expression with obesity. Moreover, beta cells exhibited higher mean EES

values, indicating enrichment in *ob/ob* islets with a commensurate reduction in alpha, delta, and PP cells (Figure 6C). Beta cells from *ob/ob* mice showed increased expression of genes involved in protein translation, secretion, and endoplasmic reticulum (ER) stress. (Figure 6D and Table S7). These genes encoded hormones and secretory granule proteins also upregulated in *KCO* mice (Figure 6E), confirming results from bulk tumor RNA-seq.

The top upregulated gene (by fold change) in *ob/ob* islets was the hormone cholecystokinin (*Cck*) (Figure 6E and Table S7). Cck is normally synthesized and secreted by enteroendocrine cells of the duodenum to induce pancreatic acinar cell zymogen release for digestion. It is dysregulated in the islets of obese mice (HFD and *ob/ob*) and has been reported to promote islet cell survival in the setting of insulin resistance, toxins, or other stresses (Lavine et al., 2015; Lavine et al., 2010). We confirmed islet Cck expression by IHC in *ob/ob* mice (Figures S5A). We further observed *Cck* expression exclusively in a subset of beta cells (Figure 6F), those of which exhibited enhanced expression of protein synthesis and secretory granule genes than their *Cck*- counterparts (Figure 6G and Table S7). Finally, *Cck* expression was inversely correlated with the expression of insulin (*Ins1* and *Ins2), Slc30a8* (a zinc transporter involved in insulin granule maturation), and the insulin-response gene *Insig1* (Figure 6H), arguing that Cck – rather than insulin – secretion may predominate in these cells.

Local islet Cck signaling drives pancreatic ductal tumorigenesis

Since exogenous administration of cerulein, a Cck analogue, promotes *Kras*-driven pancreatic tumorigenesis in mice (Guerra et al., 2007), we hypothesized that, in the setting of obesity, endogenous islet-derived Cck could drive PDAC development. Systemic Cck levels were not increased in obese mice (Figure S5B), arguing that islet Cck acts locally. Cck expression was specifically observed in islets from obese models and markedly reduced by weight loss interventions (Figures 7A-B and S5C-E), consistent with an adaptive response to obesity. We further analyzed human PDAC and observed islet expression of CCK in ~60% of samples (Figures 7C-D). Although CCK expression did not correlate with BMI (Figure 7D), cancer-associated weight loss prior to diagnosis may confound this analysis. Therefore, we procured islets from human donors without known malignancy and observed a positive relationship between BMI and CCK expression (Figure 7E). Together, these data demonstrate that obesity is associated with islet Cck expression in both mice and humans.

To test directly whether islet Cck promotes tumor progression, we utilized *MIP-Cck* transgenic mice, which exhibit beta cell-specific Cck expression comparable to *ob/ob* mice (Lavine et al., 2015). Remarkably, non-obese compound transgenic mice (*MKC:MIP-Cck; Pdx1-Cre; Kras*$^{LSL\text{-}G12D/WT}$) displayed a significant increase in tumor burden compared to *KC* controls (Figure 7F), supporting the hypothesis that islet *Cck* overexpression can function as an independent driver of pancreatic ductal tumorigenesis. Prior work has shown that the competitive Cck receptor (Cckr) antagonist proglumide, at doses that block physiologic Cck function, impedes tumor progression in non-obese *KC* mice (Smith et al., 2014). Since obesity-augmented islet Cck expression appears to function as a local driver of early PDAC progression, we anticipated that proglumide treatment should be insufficient to impair progression in the setting of supraphysiologic local concentrations of Cck in *KCO*

mice. Indeed, although proglumide induced the expected systemic pharmacodynamic effect of slowing weight gain, no significant impact on tumor development was observed (Figure S3). Thus, these data provide evidence for the importance of aberrantly-expressed pancreatic endocrine hormones beyond insulin in driving obesity-associated PDAC.

Beta cell proliferation and transcription factor signatures correlate with *Cck* expression

We next sought to explore the mechanisms of islet Cck induction *in vivo*. We hypothesized that islet stress from obesity might stimulate Cck expression to promote beta cell survival (Lavine et al., 2015). Consistent with this hypothesis, islet Cck expression was blunted in dapagliflozin-treated mice in which beta cell function was preserved (Figure S4I). We further compared the transcriptional profiles of single *Cck*+ and *Cck*− beta cells derived from *ob/ob* mice. Since islet expansion is a consequence of obesity (Linnemann et al., 2014) and beta cell division has been associated with polyhormone expression (Bocian-Sobkowska et al., 1999), we suspected that beta cell proliferation could act as a stimulus for *Cck* expression. Indeed, we observed a relative upregulation of cell cycle genes in *Cck*+ beta cells compared to their *Cck*-counterparts and an increased proportion of polyhormonal *Ins2*+/*Gcg*+ cells expressing *Cck* compared to monohormonal insulin-expressing (*Ins1*+/*Ins2*+) cells (Figures S6A-C). Recent work has suggested that islet resident macrophages may induce beta cell proliferation in the context of HFD-induced obesity via PDGF signaling (Ying et al., 2019). To evaluate for this in *ob/ob* mice, we examined *Ptprc*+ (*Cd45*+) immune cells in our islet scRNA-seq data, the majority of which expressed macrophage markers (*Cd68* and *Cd74*) (Figures S6D-E). Islet macrophages in *ob/ob* mice exhibited upregulation of genes associated with proliferation and downregulation of genes associated with cytokine signaling and inflammatory responses (Figures S6F-I), mirroring HFD-induced changes (Ying et al., 2019). These macrophages also upregulated beta cell growth factors including *Pdgfb* (Figure S6J), implicating obesity-associated changes in islet macrophages as a potential instigator of beta cell proliferation in *ob/ob* mice.

To further define molecular mechanisms that contribute to islet *Cck* expression, we examined beta cell expression of transcription factors, given their role in regulating hormone expression during islet development. Prior work has implicated Tle3/Grg3 in the suppression of *Gcg* expression in beta cells as islets develop (Metzger et al., 2014). We similarly observed decreased expression of *Tle3/Grg3* and another transcriptional co-repressor *Ehf* as the top significantly downregulated genes in *Cck*+ compared to *Cck*- cells (Figure S6K and Table S7). Furthermore, both *Tle3/Grg3* and *Ehf* expression inversely correlated with *Cck* expression in *ob/ob* beta cells (Figure S6L). Together, these data support a role for beta cell proliferation and alterations in transcription factor expression as potential drivers of islet *Cck* expression in response to obesity.

Endocrine-exocrine Cck signaling in obesity

Finally, we evaluated how Cck functions in the local microenvironment to drive tumor development. While exogenous cerulein administration is commonly used as a model for experimental pancreatitis (Guerra et al., 2007), our data support a pro-tumorigenic effect of islet Cck independent of inflammation. *MIP-Cck* mice did not exhibit overt evidence of inflammation or fibrosis (Figure S7A), even up to one year of age (Lavine et al., 2015).

Conversely, it is conceivable that local inflammation, induced by obesity, could promote islet expression of Cck. Arguing against this hypothesis, acute (cerulein- or arginine-induced) or chronic (cerulein-induced) pancreatitis did not elicit islet Cck expression in mice (Figures S7B-C). Similarly, CCK expression was not significantly observed in islets of human patients with chronic pancreatitis of varying etiologies (Figure S7D).

PDAC is commonly thought to arise from acinar or ductal cells (Kopp et al., 2012; Ray et al., 2011), suggesting that the exocrine pancreas is the target of islet Cck. Alternatively, Cck has been shown to stimulate insulin secretion from beta cells in mice (Lo et al., 2011), which in turn could modulate early tumorigenesis. Contrary to this latter hypothesis, Cck receptor (*Cckar* or *Cckbr*) transcripts were detectable in <0.05% of beta cells (compared to 12% of *Prss2*+/*Cela1*+ acinar cells) profiled from wild-type and *ob/ob* mice by scRNA-seq at our depth of sequencing. Furthermore, *MIP-Cck* mice do not exhibit increased insulin release during fasting or following glucose stimulation (Lavine et al., 2015), and *ob/ob* islets were impaired in glucose-stimulated insulin secretion (Figures S4B-D). Thus, we conclude that endocrine-derived Cck likely acts on acinar cells to drive tumorigenesis.

Evidence supports a direct effect of Cck on acinar cells in rodent models to induce zymogen secretion and proliferation (Kanemitsu et al., 2006; Logsdon, 1986). Although CCKR expression in human acinar cells is lower than observed in rodents, recent studies argue for a similar direct effect of CCK on intracellular signaling and zymogen release in primary human acinar cells (Liang et al., 2017; Murphy et al., 2008). Cck is thought to promote tumor formation through proliferative acinar cell regeneration and/or acinar cell reprogramming leading to acinar-to-ductal metaplasia (ADM), a prerequisite step in acinar cell-derived PDAC development (Kopp et al., 2012; Storz, 2017). Cerulein is capable of directly stimulating ADM in acinar explant cultures (Ardito et al., 2012). Furthermore, we observed an increase in Ki67+ acinar cells in *MKC* mice compared to *KC* controls (Figure S7E), consistent with enhanced islet Cck-induced acinar cell proliferation. Together, these data support a model in which obesity-induced islet Cck expression cooperates with oncogenic *Kras* to drive tumorigenesis via acinar cell proliferation and ductal transformation (Figure 7G).

DISCUSSION

In this study, we demonstrate that obesity plays a causal and reversible role in early PDAC progression in mice. Molecular analyses link obesity to changes in the local microenvironment and tumorigenesis via adaptive endocrine-exocrine signaling by pro-tumorigenic hormones. Hormones have long been postulated as contributing to obesity-associated cancers with principal mechanisms including dysregulation of 1) islet-derived insulin or insulin-like growth factor 1 (IGF1); 2) adipocyte secreted factors (adipokines) including leptin and adiponectin; and 3) steroid sex hormones (Murphy et al., 2018; Ulrich et al., 2018). Of these mechanisms, epidemiologic studies support a role for both insulin/IGF1 and adipokines in PDAC development, as elevated levels of insulin, proinsulin, and leptin and low levels of IGF binding protein-1 and adiponectin are associated with increased PDAC risk (Babic et al., 2016; Bao et al., 2013a; Bao et al., 2013b; Wolpin et al., 2013; Wolpin et al., 2007). Though previous studies suggested that leptin can promote PDAC

proliferation (Harbuzariu et al., 2017; Mendonsa et al., 2015), our observation of accelerated tumorigenesis in obese mice deficient in leptin signaling (Figures 1 and S1A-B) supports a leptin-independent mechanism for obesity in tumor progression. Furthermore, the capacity for caloric restriction to intercept progression in *KCO* mice (Figures 2E-F) is consistent with obesity, rather than dysregulation of leptin signaling or the associated physiologic response to starvation (Friedman, 2019), as a driver of PDAC development.

Apart from insulin (Wang et al., 2018; Zhang et al., 2019), *in vivo* evidence for a pro-tumorigenic role of pancreatic islet hormones is limited. Our study identifies obesity-associated aberrant islet *Cck* expression as a cancer driver through a local effect in the pancreas. Ultrastructural and perfusion studies endorse the existence of an islet portal system perfusing exocrine cells (the islet-acinar axis) (Barreto et al., 2010; Williams and Goldfine, 1985). Alternatively, capillary leak or neovascularization in the setting of islet cell expansion and local tissue injury from early developing tumors may alter blood flow and permit high concentrations of islet-derived Cck to access exocrine cells. The significance of obesity-driven islet adaptations is highlighted by the observation that *Cck*+ beta cells show diminished expression of genes involved in insulin secretion, including insulin itself (Figure 6H), consistent with major alterations in the secretome. We further demonstrate that CCK is expressed in islets in human PDAC (Figure 7C) and that islet CCK expression correlates with BMI (Figure 7E), supporting the possibility that a similar phenomenon occurs in human PDAC development. Our findings add to the growing body of evidence that obesity may be pro-tumorigenic through its microenvironmental rather than systemic consequences (Olson et al., 2017). Although evidence supporting a role for Cck signaling in PDAC progression exists (Nadella et al., 2018; Smith et al., 2014; Smith and Solomon, 2014), prior studies focused on intestinal-derived Cck, the physiologic source of systemic Cck. On the contrary, our work highlights a local source of Cck – induced by obesity within the pancreas itself – and offers the first example of endocrine-exocrine signaling beyond insulin in PDAC development.

Our results also demonstrate that weight loss impedes the elaboration of pro-tumorigenic hormonal adaptations – including islet Cck expression – and early PDAC progression. These data are consistent with human cohort studies showing that bariatric surgery reduces cancer incidence, including for pancreatic cancer (Schauer et al., 2019; Xu et al., 2018). In addition to weight loss, we explored alternative mechanisms that may influence islet adaptation. Specifically, we identified beta cell proliferation and changes in the expression of transcription factors known to govern islet hormone expression as highly associated with islet *Cck* expression (Figure S6). We suspect that islet glucotoxicity (Weir, 2020) may induce Cck expression as an adaptive survival response, given the capacity of Cck to maintain islet cell survival in the setting of stress (Lavine et al., 2015). Accordingly, our data show that glucose lowering and the resultant preservation of beta cell function by SGLT2 inhibition are associated with reduced tumor progression and islet Cck expression (Figures S4F-I). Nonetheless, the precise mechanisms by which obesity induces these islet adaptations, including Cck elaboration, remain to be fully elucidated. Future studies towards this aim may offer additional strategies beyond weight loss for PDAC prevention.

STAR METHODS

LEAD CONTACT AND MATERIALS AVAILABILITY

Further information and requests for resources and reagents should be directed to and will be fulfilled by the Lead Contact, Mandar Deepak Muzumdar (mandar.muzumdar@yale.edu). All unique/stable reagents generated in this study are available from the Lead Contact with a completed Materials Transfer Agreement.

EXPERIMENTAL MODEL AND SUBJECT DETAILS

Animals studies—Animal studies were approved by the Massachusetts Institute of Technology (MIT) and Yale University Institutional Animal Care and Use Committees (IACUC). *ob* (Stock #000632), *db* (Stock #000697), *Pdx1-Cre* (Stock #014647), $p53^{fl/fl}$ (Stock #008462), *MADM11-GT* (Stock #013749), *MADM11-TG* (Stock #013751), and *C57BL/6J* (Stock #000664) mice were obtained from the Jackson Laboratory. *MIP-Cck* mice (Lavine et al., 2015) were obtained from D. B. Davis of the University of Wisconsin. $Kras^{LSL\text{-}G12D}$, $p53^{R172H/WT}$, $p53^{KO/WT}$, and $Kras^{LA2}$ (a “hit-and-run” allele that results in spontaneous activation of oncogenic *Kras*) mice were generated previously by the Jacks lab (Jacks et al., 1994; Jackson et al., 2001; Johnson et al., 2001; Olive et al., 2004). *Pdx1-Cre;* $Kras^{LSL\text{-}G12D/WT}$*(KC), KC; ob*/+ and *KC; ob/ob (KCO), KC; db/+, KC; db/db,* $Kras^{LA2}$; +/+, and $Kras^{LA2}$; *ob/ob* were produced by intercrossing mice with the appropriate alleles. *KPC* mice, including *KC;* $p53^{R172H/WT}$; *KC;* $p53^{fl/WT}$, *KC;* $p53^{R172H/fl}$, *KC;* $p53^{fl/fl}$, and *KC; MADM11-GT,*$p53^{WT}$/*MADM11-TG-*$p53^{KO}$ (*MADM-p53*), were generated as described previously (Muzumdar et al., 2016). Mice were genotyped by PCR using template tail DNA isolated by the HotShot method and GoTaq Green Mastermix (Promega). Genotyping primers and protocols have been previously reported (Ellett et al., 2009; Lavine et al., 2015; Muzumdar et al., 2016) or are available online (http://www.jax.org).

Adult animals of both genders were used in all experiments except for islet isolation studies in which only males were used. Specific developmental age of mice used is listed in figure legends. Mice were housed in a specific-pathogen free facility, kept at room temperature with standard day-night cycles, and maintained on a mixed background unless otherwise specified. Animals were monitored at least weekly for signs of morbidity and were euthanized by CO2 asphyxiation when they met euthanasia criteria. Date of euthanasia relative to birth date was used for Kaplan-Meier survival analyses.

For diet studies, $Kras^{LA2}$ mice were started on high-fat (60% kcal fat, Research Diets 12492) or low-fat (10% kcal fat, Research Diets 12240J) diets at 4 weeks of age. For caloric restriction, mice were fed 1 gram of normal chow per mouse per day, as previously described (Skowronski et al., 2017). For drug studies, *KCO* mice were treated with pharmaceutical-grade aspirin (2 mg/mL, Spectrum Chemical), metformin (2 mg/mL, Spectrum Chemical), proglumide (0.1 mg/mL, Sigma), or dapagliflozin (0.02 mg/mL, MedChem Express) in drinking water starting at 6 weeks of age and treated for 6 weeks continuously. Water consumption was measured weekly when treated water was replaced. *KCO* mice drank 7.69 +/− 0.58 (s.d.), 8.95 +/− 2.24, 8.09 +/− 3.21, 9.70 +/− 1.49, 8.97 +/− 3.98 mL drinking water daily for untreated (control), aspirin, metformin, proglumide, and

dapagliflozin, respectively. Water intake was not statistically different from control for each treatment condition (two-tailed student's t-test).

Based on water consumption, average daily doses were 17.9, 16.2, 0.97, and 0.18 mg for aspirin, metformin, proglumide, and dapagliflozin, respectively, leading to an average daily dose exposure of ~456, 436, 26 mg/kg, and 4.7 mg/kg, in-line with prior studies using these agents (Chandel et al., 2016; Saponaro et al., 2019; Smith et al., 2014). Mice were randomized following pre-stratification for gender in all treatment conditions. Weights were monitored using a standard small animal scale. Glucose was measured on a OneTouch Ultra2 glucometer on whole blood collected by tail clip. For serum studies, whole blood was collected from anesthetized mice by retro-orbital bleed or terminal cardiac puncture, allowed to clot for 30 minutes at room temperature, and spun through a serum separator tube (Sarstedt) at 10,000 rpm for 5 min prior to storage at −80°C or analysis. Serum Cck was measured by EIA (RayBiotech, Cat# EIAM-CCK). Serum insulin (RIA, Linco Cat# RI-I3K) and C-peptide (ELISA, Alpco Diagnostics Cat# 80-CPTMS-E01) were measured by the Yale Diabetes Research Core.

Cell line derivation, culture, and treatments—Murine *KPC* PDAC (mPDAC) cell lines (7307 and 7310) were isolated from primary autochthonous pancreatic tumors arising in female C57/B6 *KC; $p53^{R172H/WT}$* mice (Hingorani et al., 2005). Tumors were enzymatically dissociated using a mix of collagenase IV, dispase, and DNAse I (Worthington) at 37°C for 30 minutes with further mechanical dissociation using a gentleMACS dissociator (Miltenyi Biotec). Cell suspensions were passed through a 100 μM filter, washed, and plated in complete media containing DMEM (Corning), 10% FBS (Thermo Fisher Scientific), and penicillin/streptomycin (Thermo Fisher Scientific). Cells were grown in standard culture conditions (37°C; 5% CO_2) for at least five passages to separate tumor cells from tumor-associated fibroblasts. For signaling studies, cells were grown in serum-free conditions overnight, treated with 100 ng/mL recombinant murine leptin (R&D Systems, Cat# 498-OB) in serum-free media, and lysed for protein analysis after 20 minutes (peak induction of downstream signaling). Viability was assessed 72 hours after treatment using the CellTiter Glo (CTG) assay (Promega).

To generate leptin receptor knockout clones, a single guide RNA (sgRNA) sequence (5'-TGAAAGCCACCAGACCTCGA) targeting exon 8 of the murine leptin receptor (LepR) was ligated into the BsmBI site in *lentiGuide-Puro* (Addgene 52963) with compatible annealed oligos to generate *lentiGuide-Puro-sgLepR*. Lentivirus for *lentiGuide-Puro-sgLepR* and *lentiCas9-blast* (Addgene 52962) were produced by co-transfection of 293T cells (grown in the same culture media and conditions as mPDAC cells above) with plasmids containing the lentiviral backbone, packaging vector (psPAX2), and envelope (VSV-G) using TransIT-LT1 (Mirus Bio). Supernatant was collected at 48 and 72 hours and applied to target cells with 8 μg/mL polybrene (EMD Millipore) for transduction. Transduced cells were treated with 10 μg/mL blasticidin S (Thermo Fisher Scientific) and 2 μg/mL puromycin (Life Technologies) for 7 days. Cells were then sorted into single cells by limiting dilution into 96-well plates to isolate clones. Knockout clones were confirmed by genomic DNA extraction using QuickExtract DNA extraction solution (Epicentre), PCR amplification of the target locus (forward primer: 5'-GGTTCTCAGTGCACGCATTT-3 '; reverse primer: 5 '-

ACAACGATTTTCCTGGCATCT-3') with Q5 polymerase (NEB), and Sanger sequencing of PCR products by the Keck Biotechnology Resource Laboratory at Yale. KO1 clone harbored two frameshift mutant alleles: a 32 bp deletion and an 18 bp deletion with a 2 bp insertion (effective 16 bp deletion). KO2 clone also harbored two independent frameshift mutant alleles: a 1 bp deletion and a 13 bp deletion.

Human biospecimen acquisition

Acquisition of resected PDAC biospecimens including institutional review board approval and informed consent procedures were previously described (Qian et al., 2018). 108 human islets of northern European descent were isolated at the Oxford Consortium for Islet Transplantation (OXCIT, Oxford, UK) as previously described (Cross et al., 2012). All studies were approved by the University of Oxford's "Oxford Tropical Research Ethics Committee" (OxTREC Reference: 2-15), or the Oxfordshire Regional Ethics Committee B (REC reference: 09/H0605/2). All organ donors provided informed consent for use of pancreatic tissue in research. Human chronic pancreatitis (etiologies included pancreatic divisum (n=5), Sphincter of Oddi dysfunction (n=2), idiopathic (n=5)) specimens were obtained from 12 adults (ages 25-60, M:F 4:8) undergoing Total Pancreatectomy and Islet Auto-Transplant (TP-IAT) program at the University of Minnesota Medical Center. Pancreatic biopsies were obtained at the time of surgery and processed for routine histologic analyses. Informed consent was obtained from all patients, and the research protocol was reviewed and approved by the University of Minnesota Institutional Review Board.

METHOD DETAILS

Mouse tissue preparation and histology—Mice were euthanized by CO2 asphyxiation and tissue was dissected, fixed in 10% neutral-buffered formalin overnight, and dehydrated in 70% ethanol prior to paraffin embedding. Adjacent 5-μm sections were cut and stained with hematoxylin and eosin or picosirius red or subject to immunohistochemistry (IHC). Primary antibodies for IHC are listed in the Key Resource Table. Mach 2 HRP-labeled micro-polymers (Biocare Medical) were used for primary antibody detection using a Thermo Scientific Autostainer 360. Slides were imaged with a modified Nikon T2R inverted microscope (MVI), 4x/10x/20x/40x objectives, and a 2.8 MP CoolSNAP Dyno CCD camera (Photometrics). Monochromatic red, green, and blue images were merged using ImageJ software (NIH).

Adeno-associated virus generation—Total RNA was isolated from flash frozen adipose tissue derived from *db/db* mice using Trizol (Ambion) and reverse transcribed with a High-Capacity cDNA Reverse Transcription kit (Thermo Fisher Scientific). Murine leptin cDNA was PCR amplified with Primestar high-fidelity PCR mix (Takara) using primers (forward 5'- ATGTGCTGGAGACCCCTGT-3', reverse 5'-TCAGCATTCAGGGCTAACATCCAACT-3') synthesized by the Koch Institute Swanson Biotechnology Center. Amplified leptin cDNA was cloned into the XhoI and NotI sites of the AAV2 backbone vector (*pFBAAVCAGmcsBgHpa*) provided by the University of Iowa Viral Vector Core (UIVVC), which generated AAV2/1CAGmLeptin (AAV-Leptin) using a baculovirus system. eGFP, cloned into the same AAV2 plasmid vector (AAV2/1CAGeGFP, AAV-GFP), was purchased from UIVVC. AAV-induced leptin expression was verified in

293T cells by western blotting 48 hours after infection. $1x10^{11}$ AAV viral particles were administered to mice via a single injection in the tibialis anterior muscle and circulating leptin levels were measured in the serum by ELISA (Crystal Chem Cat# 90030).

Immunoblotting—Cells were lysed with ice-cold RIPA buffer (Thermo Fisher Scientific), supplemented with 0.5 μM EDTA and Halt protease/phosphatase inhibitor cocktail (Thermo Fisher Scientific), rotated at 4°C for 15-30 minutes to mix, and centrifuged at maximum speed for 15 minutes to collect whole cell lysates. Protein concentration was measured with the BCA protein assay (Pierce). 30 μg of total protein per sample was loaded into 4-12% NuPAGE Tris-Bis (Thermo Fisher Scientific) or 4-20% Tris-Glycine TGX (Bio-Rad) gradient gels and separated by SDS-PAGE. Proteins were transferred to nitrocellulose (for fluorescence detection) or PVDF (for chemiluminescent detection) membranes and blocked with Odyssey Blocking Buffer (LI-COR) or 5% milk, respectively. Primary antibodies used for immunoblotting are listed in the Key Resource Table. HSP90 and beta-tubulin were used as loading controls. Primary antibodies were detected with fluorescent DyLight-conjugated (Cell Signaling Technology) or HRP-conjugated (Jackson Immunoresearch) secondary antibodies for fluorescent (LI-COR Odyssey scanner) or chemiluminescent detection (Perkin Elmer ECL), respectively. Quantification of phosphorylated protein levels was performed using Image Studio Lite (LI-COR) and normalized to total protein levels analyzed on the same membrane.

DNA and RNA isolation from mouse tumors—Mice were euthanized by cervical dislocation and pancreata were rapidly dissected, flash frozen in liquid nitrogen, and stored at −80C. Prior to DNA and RNA isolation, frozen tumors were mechanically ground in liquid nitrogen using a mortar and pestle. Genomic DNA and total RNA were extracted from ground tumor tissue using a Qiagen Allprep DNA/RNA mini kit per manufacturer's instructions. DNA concentration was measured using Quant-iT Picogreen dsRNA Assay Kit (Thermo Fisher Scientific). RNA concentration, quality, and purity were determined using an Agilent Bioanalyzer.

Mouse tumor exome sequencing and analysis—Exome capture on mouse tumor genomic DNA was performed by Macrogen Corp. using an Agilent SureSelectXT Mouse All Exon kit. 100-nt paired-end sequencing to a raw sequence depth of 150X per sample on a HiSeq 2500 (Illumina) was subsequently performed. Variant calls were made using an approach similar to the HaJaVa platform (McFadden et al., 2016). Reads were processed to remove adapter sequences (using exact matches to 10-mer adapter start sequence: AGATCGGAAG) using the FASTX-toolkit (http://hannonlab.cshl.edu/fastx_toolkit). Surviving reads greater than or equal to 15-nt in length were retained. Reads were aligned to the mouse mm9 genome assembly (UCSC) using BWA (v0.5.5). Duplicates were removed using Picard (v1.21) MarkDuplicates utility. Local realignment of reads around indels and base quality recalibration were performed using GATK (v1.0.5538). Variant calls were made with GATK UnifiedGenotyper using the mm9 reference sequence in regions targeted by the Agilent capture kit (version G7550_20110119_mm9 from Agilent). Calls with at least 14X read coverage and dual strand support were retained and further filtered using GATK VariantFiltration (arguments - clusterWindowSize 10 -cluster 3), GATK SelectVariants

(arguments "SB < −0.1", "QUAL >= 30.0", "QD >= 5.0", "HRun <= 5"), and Sanger Mouse Genomes Project Variant calls (Keane et al., 2011). Variants were annotated using Annovar (Wang et al., 2010) (version 2016Feb01) and mouse dbSNP build 142 (ftp.ncbi.nlm.nih.gov/snp/).

Mouse tumor RNA sequencing and analysis—cDNA libraries from tumor total RNA were prepared by the MIT BioMicro Center using the Neoprep library preparation system (Illumina) with indexed adaptor sequences and polyA selection. Sequencing was performed on an Illumina NextSeq to obtain paired-end 75-nt reads. All reads that passed quality metrics were mapped to UCSC mm9 mouse genome build (http://genome.ucsc.edu/) using RSEM (v1.2.12) (http://deweylab.github.io/RSEM/). All RNA-seq analyses were conducted in R. High-resolution signature analyses between tumors from obese (*KCO* and *KCO* treated with AAV-GFP) and non-obese (*KC* and *KPC*) models were performed using a blind source separation methodology based on Independent Component Analysis (ICA), as previously described (Hyvarinen and Oja, 2000; Muzumdar et al., 2017). Z-scores for each tumor for each component (signature) were calculated using ICA and reflect relative correspondence between a tumor and each signature (degree of positive or negative correlation). 3 derived signatures (Sig6, Sig12, and Sig13) showed statistically significant differences in Z-scores comparing *KCO* and *KC/KPC* tumors ($p<0.01$, Mann-Whitney test) and were used in subsequent analyses.

Gene Set Enrichment Analyses (GSEA) (http://software.broadinstitute.org/gsea/) were carried out using standardized signature correlation scores (for ICA signatures) with default settings. Normalized enrichment score (NES), false discovery rate (FDR), ICA signature (Sig6, Sig12, or Sig13 separating *KCO* and *KC/KPC* tumors), and MSigDB gene set rank are shown in relevant figures. Network representations of GSEA results were generated using EnrichmentMap (http://www.baderlab.org/Software/EnrichmentMap) for Cytoscape v3.3.0 (http://www.cytoscape.org) with $p<0.005$ and $FDR<0.1$. Each circle represents a gene set with circle size corresponding to gene set size and intensity corresponding to enrichment significance. Red is upregulated and blue is downregulated. Each line corresponds to minimum 50% mutual overlap with line thickness corresponding to degree of overlap. Cellular processes for gene set clusters were manually curated.

Genes with standardized signature correlation scores $z > 3$ (or $z < -3$) in Sig6, Sig12, and Sig13 were used as gene sets to stratify TCGA (https://tcga-data.nci.nih.gov/tcga/) Pancreatic Adenocarcinoma (PAAD) tumors (TCGA Research Network, 2017) using ssGSEA (Barbie et al., 2009). Associated patients within top and bottom buckets (> or < 1 s.d.) were each assessed for over-representation of previously established molecular subtypes (squamous (n=31), immunogenic (n=28), progenitor (n=53), ADEX (n=38) (Bailey et al., 2016)) using the hypergeometric test. The human tumor subtype classifications used are based on those reported by TCGA (TCGA Research Network, 2017) prior to tumor cellularity correction.

Tumor suppressor gene mutations in RNA-seq datasets were called using the GATK Best Practices workflow for SNP calling on RNA-seq data (software.broadinstitute.org/gatk/documentation/article.php?id=3891). Transcriptomic reads were trimmed to eliminate

adapter sequences using an exact 10-mer match to the start of the adapter sequence (AGATCGGAAG) using Cutadapt (v1.16) and subsequently mapped to the mouse mm9 (UCSC) genome assembly using the STAR RNA-seq aligner with default parameters. Picard v2.17.0 MarkDuplicates utility was used to mark duplicates in the aligned data. GATK (v3.8.0) toolkit was used to "SplitNTrim" and reassign mapping qualities as per GATK best practices. Indel realignment and base recalibration were performed as recommended. Variants were called against the mm9 reference sequence using the GATK HaplotypeCaller and filtered using GATK VariantFiltration with recommended parameters. Variant calls were annotated using Annovar (version 2016Feb01).

Evaluation of cancer driver genes in human PDAC—Targeted exome sequencing and IHC of human PDAC biospecimens has been previously described (Qian et al., 2018). Pre-operative body-mass index (BMI) and molecular data on the main PDAC driver genes was available for 184 of 356 patients from this prior study. Of note, PDAC patients experience significant weight loss in the months preceding diagnosis, and weight at surgery may therefore not be fully reflective of weight in the prediagnostic period. In 125 patients with available weight data at 6 months before diagnosis, we compared weight at surgery with weight 6 months before diagnosis, and observed a strong correlation (Spearman's rank correlation coefficient = 0.90, $p<0.0001$). This suggests that although weight may decrease in months preceding diagnosis, the rank order of 2 measurements is likely to be highly consistent. We used World Health Organization categories to classify patients as normal weight (<25 kg/m^2), overweight (25-30 kg/m^2), or obese (>30 kg/m^2). Using SAS software (SAS Institute, Inc., Version 9.4), we performed logistic regression adjusted for age at surgery (continuous), gender (men, women), study site, grade (well/moderately differentiated, poorly differentiated/undifferentiated, unknown), perineural invasion (no, yes, unknown), lymphovascular invasion (no, yes, unknown), N stage (N0, N1, unknown), T stage (T1/T2, T3/T4, unknown), and tumor location (head/uncinate, body, tail, unknown), to evaluate the association between BMI (normal, overweight, obese) and driver alterations in human PDAC. We calculated odds ratios (ORs) and 95% confidence intervals (CIs). We used the Kruskal-Wallis test to compare the number of driver alterations across BMI categories.

Murine islet GSIS studies—Islets from C57/B6 wild-type and *ob/ob* male mice (n=4 mice/group) were isolated and perifused for glucose stimulated insulin secretion (GSIS) studies as previously described (Jesinkey et al., 2019) with a few minor changes, which are noted. Isolated islets were recovered overnight and were perfused the following day in DMEM (D5030, Sigma) supplemented with 24 mM $NaHCO_3$, 10 mM HEPES, 2.5 mM glucose, 2 mM glutamine, and 0.2% BSA. The islets first equilibrated for 1 hour at 2.5 mM glucose on the perifusion instrument. After the stabilization period, islets were perfused with basal (2.5 mM) glucose for 10 minutes followed by stimulatory glucose (16.7 mM) for 45 minutes. After stimulation with glucose, the islets were exposed to basal glucose for 15 minutes followed by a final 30 mM KCl step to ensure that the insulin secreting machinery distal to mitochondrial metabolism was intact in the two groups tested. During the perifusion, eluent was collected into a 96-well plate format and both secreted and total islet

insulin concentrations were determined by a Mouse High Range Insulin ELISA assay kit (Alpco Diagnostics) and normalized to islet DNA using Picogreen.

Single-cell RNA sequencing of mouse islets—Murine pancreatic islets used for single-cell analysis were isolated as described for GSIS studies, except samples were dispersed into single cells immediately after isolation using accutase (Gibco) and resuspended in 1 mL of PBS. Dead cells were removed using a MACS Dead Cell Removal Kit (Miltenyi Biotec) and cell concentration determined using a Countess II Automated Cell Counter (Thermo Scientific). Single-cell library preparation was performed using a Chromium Single Cell 3' Reagent Kit v3 (10X Genomics) and sequenced by Illumina HiSeq. Gene counts matrices were generated using CellRanger. Genes detected in fewer than 15 cells were removed and cells with library sizes greater than 15,000 UMI/cell were removed as potential doublets. We observed a bimodal distribution of mitochondrial gene detection and removed cells in the top 12.5% of library-size normalized mitochondrial expression as apoptotic cells. We then focused our analysis on single-hormone expressing islet cells as measured by the expression of *Ins1/Ins2, Gcg, Sst*, and *Ppy*, removing dual hormone-expressing cells and cells expressing markers of acinar, ductal, endothelial, or immune cells.

Cells were visualized using PHATE (Moon et al., 2019) with default parameters and gene expression was denoised using MAGIC (van Dijk et al., 2018) with default parameters. The Enhanced Experimental Signal (EES) was calculated using MELD (Burkhardt et al., 2019) with default parameters. Overlap of upregulated/downregulated genes comparing *ob/ob* vs. wild-type (WT) ($q<0.0001$, log2FC>0.5, mean normalized expression counts >0.5) or *Cck*+ (expression>0) vs. *Cck*- ($q<0.0001$, mean normalized expression counts > *Cck*) beta cells with gene ontology (C5 biological process and cellular components) and hallmark (H) gene sets in MSigDB (http://software.broadinstitute.org/gsea/) were computed using the hypergeometric test. Statistical testing for differential expression was performed using the Mann-Whitney U test as implemented in diffxpy.

CCK evaluation in human biospecimens—IHC for detection of CCK expression in human PDAC samples was performed on 4-μm sections of formalin-fixed paraffin-embedded tissue blocks containing neoplastic and non-neoplastic pancreatic parenchyma that were obtained as part of specimens resected for PDAC treatment, as previously described (Qian et al., 2018). Antigen retrieval was performed using citrate buffer (pH 6.0, Dako) in a 2100 Antigen Retriever system (Electron Microscopy Sciences). Sections were then incubated with dual endogenous peroxidase block (Dako) for 20 minutes at room temperature, protein block (Dako) for 10 minutes at room temperature, and anti-CCK8 primary antibody for 1 hour at 4°C. Chromogenic visualization was subsequently performed using the EnVision+ System- HRP (Dako) with a 3 minute diaminobenzidine (DAB) incubation followed by counterstaining with hematoxylin. For evaluation of CCK expression, the surrounding exocrine pancreas served as an internal negative control. If present within the section, neuroendocrine cells within the epithelium of the duodenum served as internal positive controls. The immunohistochemical assessment of CCK expression was conducted without knowledge of BMI or other patient data.

For human donor islets, RNA was extracted, sequenced, and analyzed as previously described (van de Bunt et al., 2015). Reads per kilobase of *CCK* transcript per million mapped reads (RPKM) was log2 normalized for analysis. For a subset of donors, BMI was not available, and samples could not be used in analysis. Given limited sample size, low and high BMI groups were specified based on the median United States BMI (28.2 kg/m^2) defined by the most recent 2015-2016 National Health and Nutrition Examination Survey (NHANES) (https://www.cdc.gov/nchs/nhanes/index.htm). This also closely approximated median BMI in the donor cohort of 28 kg/m^2.

Induction of murine pancreatitis—Acute pancreatitis was induced in adult C57/B6 mice (~25 grams in weight) using cerulein (Sigma; six hourly 50 μg/kg intraperitoneally (IP) injections) or arginine (Sigma; three hourly 3 g/kg IP injections). Mice were euthanized and processed for histology at 12 and/or 48 hours after the first injection. Chronic pancreatitis was induced in adult C57/B6 mice with cerulein given six hourly 50 μg/kg IP injections three times a week for 2 weeks prior to analysis. Acute or chronic PBS-treated mice were used as controls. Two mice from each treatment group were analyzed.

QUANTIFICATION AND STATISTICAL ANALYSIS

Percentage of tumor burden was quantified blinded to group on scanned slides (Aperio) by measuring cross-sectional tumor area (PanIN or PDAC including stroma) relative to total pancreas area using ImageJ or QuPath v0.1.2 software. Details of statistical tests used for each experiment including n, definition of center, and precision measures are described in the figure legends. All error bars denote standard error of mean (s.e.m.) unless otherwise denoted. A p-value of <0.05 was used to denote statistical significance. In general, p-values for comparisons of two groups were determined by two-tailed student's t-test (for normally distributed data) or Mann-Whitney U test (for non-parametric data), as noted in the figure legends, using Prism (Graphpad). The log-rank test was used for Kaplan-Meier survival analyses using Prism. All replicates were included in these analyses and represent measurements from distinct samples (biologic replicates) unless otherwise noted in the figure legends.

DATA AND CODE AVAILABILITY

The datasets generated and/or analyzed during the current study are available in the NCBI Sequencing Read Archive (SRA) under accession number PRJNA544740 and the NCBI Gene Expression Omnibus (GEO) under accession numbers GSE131714 and GSE137236. Primary murine PDAC cell lines and constructs are available upon request. Python scripts for scRNA-seq analyses are available on GitHub (https://github.com/KrishnaswamyLab). Computer code for RNA-seq signature analysis (ICA) will be made available upon request. Other software tools (including version numbers) for exome and RNA-seq analyses are listed above or referenced.

Supplementary Material

Refer to Web version on PubMed Central for supplementary material.

ACKNOWLEDGEMENTS

We thank F. Gorelick, M. Lemmon, and F. Wilson for critical reading of the manuscript; K. Mercer for technical assistance; K. Cormier and C. Condon from the Hope Babette Tang (1983) Histology Facility of the Koch Institute Swanson Biotechnology Center and A. Brooks, P. Gaule, Y. Bai, B. Acs, and D. Rhim from Yale Pathology Tissue Services for histology assistance; M. Robert and R. Bronson for pathology assistance; S. Levine, V. Dayal, and J. Penterman from the MIT BioMicro Center for bulk RNA-seq support; J. Heitke, G. Wang, C. Castaldi, and S. Mane from the Yale Center for Genome Analysis for assisting with scRNA-seq; the University of Iowa Viral Vector core for AAV constructs and generation; M. Batsu and R. Jacobs from the Yale Diabetes Research Core for serum ELISA/RIA studies; the Oxford Human Islet Isolation facility for the provision of human islets for research; T. Kolodecik and F. Gorelick for providing murine pancreatitis specimens; F. Zheng for CRISPR constructs; and A. Berns, D. B. Davis, A. Lowy, L. Luo, and Jackson Laboratories for mice.

This work was supported in part by a Lustgarten Foundation Research Investigator Grant (C.S.F. and M.D.M.), Cancer Center Support (core) grants P30-CA016359 (C.S.F.) and P30-CA014051 (T.J.) from the National Cancer Institute, a Pilot Grant from the Yale Cancer Center (M.D.M.), a Yale Cancer Innovations Award (M.D.M.), and an NIH Director's New Innovator Award (DP2-CA248136) (M.D.M.). The National Institute for Health Research, Oxford Biomedical Research Centre funded islet provision. C.G. is funded by the NIH/NIGMS (T32-GM007499). D.B.B. is funded by the NICHD (F31-HD097958). A.B. is funded by the NCI (K07-CA222159) and a Bob Parsons Fellowship. A.L.G. received support as a Wellcome Senior Fellow in Basic Biomedical Science with funding in Oxford by the Wellcome Trust (095101, 200837, 106130, 203141), Medical Research Council (MR/L020149/1), European Union Horizon 2020 Programme (T2D Systems), and the NIDDK (U01-DK105535, U01-DK085545). M.I.M. received support as a Wellcome Senior Investigator and an NIHR Senior Investigator. Relevant funding support for this work came from Wellcome (090532, 098381, 212259) and the NIHR (NF-SI-0617-10090). The views expressed in this article are those of the author(s) and not necessarily those of the NHS, the NIHR, or the Department of Health. R.G.K. is funded by the NIDDK (P30-DK045735, R01-DK110181) and a Yale Cancer Innovations Award. S.K. is funded by the NIH (R01-GM130847), HIPC (2U19AI089992), and the Chan Zuckerberg Initiative (CZF2019-002440). B.M.W. acknowledges support from the Hale Family Center for Pancreatic Cancer Research, Lustgarten Foundation, NIH (U01-CA210171), Stand Up to Cancer, Noble Effort Fund, Wexler Family Fund, and Promises for Purple. T.J. is a Howard Hughes Medical Institute Investigator, the David H. Koch Professor of Biology, and a Daniel K. Ludwig Scholar. M.D.M. is supported by the NCI (K08-CA2080016) and was supported by a Conquer Cancer Foundation-American Society for Clinical Oncology (CCF-ASCO) Young Investigator Award and the NIH Loan Repayment Program. The content is solely the responsibility of the authors and does not necessarily represent the official views of the National Institutes of Health.

REFERENCES

Ardito CM, Gruner BM, Takeuchi KK, Lubeseder-Martellato C, Teichmann N, Mazur PK, Delgiorno KE, Carpenter ES, Halbrook CJ, Hall JC, et al. (2012). EGF receptor is required for KRAS-induced pancreatic tumorigenesis. Cancer Cell 22, 304–317. [PubMed: 22975374]

Babic A, Bao Y, Qian ZR, Yuan C, Giovannucci EL, Aschard H, Kraft P, Amundadottir LT, Stolzenberg-Solomon R, Morales-Oyarvide V, et al. (2016). Pancreatic Cancer Risk Associated with Prediagnostic Plasma Levels of Leptin and Leptin Receptor Genetic Polymorphisms. Cancer Res 76, 7160–7167. [PubMed: 27780823]

Bailey MH, Tokheim C, Porta-Pardo E, Sengupta S, Bertrand D, Weerasinghe A, Colaprico A, Wendl MC, Kim J, Reardon B, et al. (2018). Comprehensive Characterization of Cancer Driver Genes and Mutations. Cell 173, 371–385 e318. [PubMed: 29625053]

Bailey P, Chang DK, Nones K, Johns AL, Patch AM, Gingras MC, Miller DK, Christ AN, Bruxner TJ, Quinn MC, et al. (2016). Genomic analyses identify molecular subtypes of pancreatic cancer. Nature 531, 47–52. [PubMed: 26909576]

Bao Y, Giovannucci EL, Kraft P, Qian ZR, Wu C, Ogino S, Gaziano JM, Stampfer MJ, Ma J, Buring JE, et al. (2013a). Inflammatory plasma markers and pancreatic cancer risk: a prospective study of five U.S. cohorts. Cancer Epidemiol Biomarkers Prev 22, 855–861. [PubMed: 23462920]

Bao Y, Giovannucci EL, Kraft P, Stampfer MJ, Ogino S, Ma J, Buring JE, Sesso HD, Lee IM, Gaziano JM, et al. (2013b). A prospective study of plasma adiponectin and pancreatic cancer risk in five US cohorts. J Natl Cancer Inst 105, 95–103. [PubMed: 23243202]

Barbie DA, Tamayo P, Boehm JS, Kim SY, Moody SE, Dunn IF, Schinzel AC, Sandy P, Meylan E, Scholl C, et al. (2009). Systematic RNA interference reveals that oncogenic KRAS-driven cancers require TBK1. Nature 462, 108–112. [PubMed: 19847166]

Bardeesy N, Aguirre AJ, Chu GC, Cheng KH, Lopez LV, Hezel AF, Feng B, Brennan C, Weissleder R, Mahmood U, et al. (2006a). Both p16(Ink4a) and the p19(Arf)-p53 pathway constrain progression of pancreatic adenocarcinoma in the mouse. Proc Natl Acad Sci U S A 103, 5947–5952. [PubMed: 16585505]

Bardeesy N, Cheng KH, Berger JH, Chu GC, Pahler J, Olson P, Hezel AF, Horner J, Lauwers GY, Hanahan D, et al. (2006b). Smad4 is dispensable for normal pancreas development yet critical in progression and tumor biology of pancreas cancer. Genes Dev 20, 3130–3146. [PubMed: 17114584]

Barreto SG, Carati CJ, Toouli J, and Saccone GT (2010). The islet-acinar axis of the pancreas: more than just insulin. Am J Physiol Gastrointest Liver Physiol 299, G10–22. [PubMed: 20395539]

Bocian-Sobkowska J, Zabel M, Wozniak W, and Surdyk-Zasada J (1999). Polyhormonal aspect of the endocrine cells of the human fetal pancreas. Histochem Cell Biol 112, 147–153. [PubMed: 10460468]

Burkhardt DB, Stanley JS, Perdigoto AL, Gigante SA, Herold KC, Wolf G, Giraldez AJ, van Dijk D, and Krishnaswamy S (2019). Quantifying the effect of experimental perturbations in single-cell RNA-sequencing data using graph signal processing. BioRxiv 532846.

Chandel NS, Avizonis D, Reczek CR, Weinberg SE, Menz S, Neuhaus R, Christian S, Haegebarth A, Algire C, and Pollak M (2016). Are Metformin Doses Used in Murine Cancer Models Clinically Relevant? Cell Metab 23, 569–570. [PubMed: 27076070]

Chang H-H, Moro A, Takakura K, Su H-Y, Mo A, Nakanishi M, Waldron RT, French SW, Dawson DW, et al. (2017). Incidence of pancreatic cancer is dramatically increased by a high fat, high calorie diet in KrasG12D mice. Plos One 12.

Chen K, Qian W, Jiang Z, Cheng L, Li J, Sun L, Zhou C, Gao L, Lei M, Yan B, et al. (2017). Metformin suppresses cancer initiation and progression in genetic mouse models of pancreatic cancer. Mol Cancer 16, 131. [PubMed: 28738823]

Chen PY, Muzumdar MD, Dorans KJ, Robbins R, Bhutkar A, Del Rosario A, Mertins P, Qiao J, Schafer AC, Gertler F, et al. (2018). Adaptive and Reversible Resistance to Kras Inhibition in Pancreatic Cancer Cells. Cancer Res 78, 985–1002. [PubMed: 29279356]

Cross SE, Hughes SJ, Clark A, Gray DW, and Johnson PR (2012). Collagenase does not persist in human islets following isolation. Cell Transplant 21, 2531–2535. [PubMed: 22472561]

Ellett JD, Evans ZP, Zhang G, Chavin KD, and Spyropoulos DD (2009). A rapid PCR-based method for the identification of ob mutant mice. Obesity (Silver Spring) 17, 402–404. [PubMed: 18948969]

Friedman JM (2019). Leptin and the endocrine control of energy balance. Nature Metabolism.

Guerra C, Schuhmacher AJ, Canamero M, Grippo PJ, Verdaguer L, Perez-Gallego L, Dubus P, Sandgren EP, and Barbacid M (2007). Chronic pancreatitis is essential for induction of pancreatic ductal adenocarcinoma by K-Ras oncogenes in adult mice. Cancer Cell 11, 291–302. [PubMed: 17349585]

Harbuzariu A, Rampoldi A, Daley-Brown DS, Candelaria P, Harmon TL, Lipsey CC, Beech DJ, Quarshie A, Ilies GO, and Gonzalez-Perez RR (2017). Leptin-Notch signaling axis is involved in pancreatic cancer progression. Oncotarget 8, 7740–7752. [PubMed: 27999190]

Hingorani SR, Petricoin EF, Maitra A, Rajapakse V, King C, Jacobetz MA, Ross S, Conrads TP, Veenstra TD, Hitt BA, et al. (2003). Preinvasive and invasive ductal pancreatic cancer and its early detection in the mouse. Cancer Cell 4, 437–450. [PubMed: 14706336]

Hingorani SR, Wang L, Multani AS, Combs C, Deramaudt TB, Hruban RH, Rustgi AK, Chang S, and Tuveson DA (2005). Trp53R172H and KrasG12D cooperate to promote chromosomal instability and widely metastatic pancreatic ductal adenocarcinoma in mice. Cancer Cell 7, 469–483. [PubMed: 15894267]

Hyvarinen A, and Oja E (2000). Independent component analysis: algorithms and applications. Neural Netw 13, 411–430. [PubMed: 10946390]

Incio J, Liu H, Suboj P, Chin SM, Chen IX, Pinter M, Ng MR, Nia HT, Grahovac J, Kao S, et al. (2016). Obesity-Induced Inflammation and Desmoplasia Promote Pancreatic Cancer Progression and Resistance to Chemotherapy. Cancer Discovery 6, 852–869. [PubMed: 27246539]

Jacks T, Remington L, Williams BO, Schmitt EM, Halachmi S, Bronson RT, and Weinberg RA (1994). Tumor spectrum analysis in p53-mutant mice. Curr Biol 4, 1–7. [PubMed: 7922305]

Jackson EL, Willis N, Mercer K, Bronson RT, Crowley D, Montoya R, Jacks T, and Tuveson DA (2001). Analysis of lung tumor initiation and progression using conditional expression of oncogenic K-ras. Genes Dev 15, 3243–3248. [PubMed: 11751630]

Jesinkey SR, Madiraju AK, Alves TC, Yarborough OH, Cardone RL, Zhao X, Parsaei Y, Nasiri AR, Butrico G, Liu X, et al. (2019). Mitochondrial GTP Links Nutrient Sensing to beta Cell Health, Mitochondrial Morphology, and Insulin Secretion Independent of OxPhos. Cell Rep 28, 759–772 e710. [PubMed: 31315053]

Johnson L, Mercer K, Greenbaum D, Bronson RT, Crowley D, Tuveson DA, and Jacks T (2001). Somatic activation of the K-ras oncogene causes early onset lung cancer in mice. Nature 410, 1111–1116. [PubMed: 11323676]

Jurczak MJ, Lee HY, Birkenfeld AL, Jornayvaz FR, Frederick DW, Pongratz RL, Zhao X, Moeckel GW, Samuel VT, Whaley JM, et al. (2011). SGLT2 deletion improves glucose homeostasis and preserves pancreatic beta-cell function. Diabetes 60, 890–898. [PubMed: 21357472]

Jurczak MJ, Saini S, Ioja S, Costa DK, Udeh N, Zhao X, Whaley JM, and Kibbey RG (2018). SGLT2 knockout prevents hyperglycemia and is associated with reduced pancreatic beta-cell death in genetically obese mice. Islets 10, 181–189. [PubMed: 30118626]

Kanemitsu D, Sakagami J, Motoyoshi T, Nakajima T, and Kataoka K (2006). Effects of the cholecystokinin A receptor antagonist loxiglumide on the proliferation and cell cycle time of pancreatic acinar cells in rats. Pancreas 32, 190–196. [PubMed: 16552340]

Keane TM, Goodstadt L, Danecek P, White MA, Wong K, Yalcin B, Heger A, Agam A, Slater G, Goodson M, et al. (2011). Mouse genomic variation and its effect on phenotypes and gene regulation. Nature 477, 289–294. [PubMed: 21921910]

Khalaf N, Yuan C, Hamada T, Cao Y, Babic A, Morales-Oyarvide V, Kraft P, Ng K, Giovannucci E, Ogino S, et al. (2018). Regular Use of Aspirin or Non-Aspirin Nonsteroidal Anti-Inflammatory Drugs Is Not Associated With Risk of Incident Pancreatic Cancer in Two Large Cohort Studies. Gastroenterology 154, 1380–1390 e1385. [PubMed: 29229401]

Khasawneh J, Schulz MD, Walch A, Rozman J, Hrabe de Angelis M, Klingenspor M, Buck A, Schwaiger M, Saur D, Schmid RM, et al. (2009). Inflammation and mitochondrial fatty acid beta-oxidation link obesity to early tumor promotion. Proc Natl Acad Sci U S A 106, 3354–3359. [PubMed: 19208810]

Kopp JL, von Figura G, Mayes E, Liu FF, Dubois CL, Morris J.P.t., Pan FC, Akiyama H, Wright CV, Jensen K, et al. (2012). Identification of Sox9-dependent acinar-to-ductal reprogramming as the principal mechanism for initiation of pancreatic ductal adenocarcinoma. Cancer Cell 22, 737–750. [PubMed: 23201164]

Kowalczyk MS, Tirosh I, Heckl D, Rao TN, Dixit A, Haas BJ, Schneider RK, Wagers AJ, Ebert BL, and Regev A (2015). Single-cell RNA-seq reveals changes in cell cycle and differentiation programs upon aging of hematopoietic stem cells. Genome Res 25, 1860–1872. [PubMed: 26430063]

Larsson SC, Orsini N, and Wolk A (2007). Body mass index and pancreatic cancer risk: A meta-analysis of prospective studies. Int J Cancer 120, 1993–1998. [PubMed: 17266034]

Lauby-Secretan B, Scoccianti C, Loomis D, Grosse Y, Bianchini F, Straif K, and International Agency for Research on Cancer Handbook Working, G. (2016). Body Fatness and Cancer--Viewpoint of the IARC Working Group. N Engl J Med 375, 794–798. [PubMed: 27557308]

Lavine JA, Kibbe CR, Baan M, Sirinvaravong S, Umhoefer HM, Engler KA, Meske LM, Sacotte KA, Erhardt DP, and Davis DB (2015). Cholecystokinin expression in the beta-cell leads to increased beta-cell area in aged mice and protects from streptozotocin-induced diabetes and apoptosis. Am J Physiol Endocrinol Metab 309, E819–828. [PubMed: 26394663]

Lavine JA, Raess PW, Stapleton DS, Rabaglia ME, Suhonen JI, Schueler KL, Koltes JE, Dawson JA, Yandell BS, Samuelson LC, et al. (2010). Cholecystokinin is upregulated in obese mouse islets and expands beta-cell mass by increasing beta-cell survival. Endocrinology 151, 3577–3588. [PubMed: 20534724]

Li D, Yeung SC, Hassan MM, Konopleva M, and Abbruzzese JL (2009). Antidiabetic therapies affect risk of pancreatic cancer. Gastroenterology 137, 482–488. [PubMed: 19375425]

Liang T, Dolai S, Xie L, Winter E, Orabi AI, Karimian N, Cosen-Binker LI, Huang YC, Thorn P, Cattral MS, et al. (2017). Ex vivo human pancreatic slice preparations offer a valuable model for studying pancreatic exocrine biology. J Biol Chem 292, 5957–5969. [PubMed: 28242761]

Linnemann AK, Baan M, and Davis DB (2014). Pancreatic beta-cell proliferation in obesity. Adv Nutr 5, 278–288. [PubMed: 24829474]

Linnemann AK, Neuman JC, Battiola TJ, Wisinski JA, Kimple ME, and Davis DB (2015). Glucagon-Like Peptide-1 Regulates Cholecystokinin Production in beta-Cells to Protect From Apoptosis. Mol Endocrinol 29, 978–987. [PubMed: 25984632]

Lo CM, Obici S, Dong HH, Haas M, Lou D, Kim DH, Liu M, D'Alessio D, Woods SC, and Tso P (2011). Impaired insulin secretion and enhanced insulin sensitivity in cholecystokinin-deficient mice. Diabetes 60, 2000–2007. [PubMed: 21602512]

Logsdon CD (1986). Stimulation of pancreatic acinar cell growth by CCK, epidermal growth factor, and insulin in vitro. Am J Physiol 251, G487–494. [PubMed: 3020992]

Massetti GM, Dietz WH, and Richardson LC (2017). Excessive Weight Gain, Obesity, and Cancer: Opportunities for Clinical Intervention. JAMA 318, 1975–1976. [PubMed: 28973170]

McFadden DG, Politi K, Bhutkar A, Chen FK, Song X, Pirun M, Santiago PM, Kim-Kiselak C, Platt JT, Lee E, et al. (2016). Mutational landscape of EGFR-, MYC-, and Kras-driven genetically engineered mouse models of lung adenocarcinoma. Proc Natl Acad Sci U S A 113, E6409–E6417. [PubMed: 27702896]

Mendonsa AM, Chalfant MC, Gorden LD, and VanSaun MN (2015). Modulation of the leptin receptor mediates tumor growth and migration of pancreatic cancer cells. PLoS One 10, e0126686. [PubMed: 25919692]

Metzger DE, Liu C, Ziaie AS, Naji A, and Zaret KS (2014). Grg3/TLE3 and Grg1/TLE1 induce monohormonal pancreatic beta-cells while repressing alpha-cell functions. Diabetes 63, 1804–1816. [PubMed: 24487024]

Moon KR, van Dijk D, Wang Z, Gigante S, Burkhardt DB, Chen WS, Yim K, Elzen A.v.d., Hirn MJ, Coifman RR, et al. (2019). Visualizing structure and transitions in high-dimensional biological data. Nature Biotechnology 37, 1482–1492.

Murphy JA, Criddle DN, Sherwood M, Chvanov M, Mukherjee R, McLaughlin E, Booth D, Gerasimenko JV, Raraty MG, Ghaneh P, et al. (2008). Direct activation of cytosolic Ca2+ signaling and enzyme secretion by cholecystokinin in human pancreatic acinar cells. Gastroenterology 135, 632–641. [PubMed: 18555802]

Murphy N, Jenab M, and Gunter MJ (2018). Adiposity and gastrointestinal cancers: epidemiology, mechanisms and future directions. Nat Rev Gastroenterol Hepatol 15, 659–670. [PubMed: 29970888]

Muzumdar MD, Chen PY, Dorans KJ, Chung KM, Bhutkar A, Hong E, Noll EM, Sprick MR, Trumpp A, and Jacks T (2017). Survival of pancreatic cancer cells lacking KRAS function. Nat Commun 8, 1090. [PubMed: 29061961]

Muzumdar MD, Dorans KJ, Chung KM, Robbins R, Tammela T, Gocheva V, Li CM, and Jacks T (2016). Clonal dynamics following p53 loss of heterozygosity in Kras-driven cancers. Nat Commun 7, 12685. [PubMed: 27585860]

Nadella S, Burks J, Al-Sabban A, Inyang G, Wang J, Tucker RD, Zamanis ME, Bukowski W, Shivapurkar N, and Smith JP (2018). Dietary fat stimulates pancreatic cancer growth and promotes fibrosis of the tumor microenvironment through the cholecystokinin receptor. Am J Physiol Gastrointest Liver Physiol 315, G699–G712. [PubMed: 29927319]

Olive KP, Tuveson DA, Ruhe ZC, Yin B, Willis NA, Bronson RT, Crowley D, and Jacks T (2004). Mutant p53 gain of function in two mouse models of Li-Fraumeni syndrome. Cell 119, 847–860. [PubMed: 15607980]

Olson OC, Quail DF, and Joyce JA (2017). Obesity and the tumor microenvironment. Science 358, 1130–1131. [PubMed: 29191893]

Papke B, and Der CJ (2017). Drugging RAS: Know the enemy. Science 355, 1158–1163. [PubMed: 28302824]

Philip B, Roland CL, Daniluk J, Liu Y, Chatterjee D, Gomez SB, Ji B, Huang H, Wang H, Fleming JB, et al. (2013). A high-fat diet activates oncogenic Kras and COX2 to induce development of

pancreatic ductal adenocarcinoma in mice. Gastroenterology 145, 1449–1458. [PubMed: 23958541]

Qian ZR, Rubinson DA, Nowak JA, Morales-Oyarvide V, Dunne RF, Kozak MM, Welch MW, Brais LK, Da Silva A, Li T, et al. (2018). Association of Alterations in Main Driver Genes With Outcomes of Patients With Resected Pancreatic Ductal Adenocarcinoma. JAMA Oncol 4, e173420. [PubMed: 29098284]

Rahib L, Smith BD, Aizenberg R, Rosenzweig AB, Fleshman JM, and Matrisian LM (2014). Projecting cancer incidence and deaths to 2030: the unexpected burden of thyroid, liver, and pancreas cancers in the United States. Cancer Res 74, 2913–2921. [PubMed: 24840647]

Rangarajan S, Bone NB, Zmijewska AA, Jiang S, Park DW, Bernard K, Locy ML, Ravi S, Deshane J, Mannon RB, et al. (2018). Metformin reverses established lung fibrosis in a bleomycin model. Nat Med 24, 1121–1127. [PubMed: 29967351]

Ray KC, Bell KM, Yan J, Gu G, Chung CH, Washington MK, and Means AL (2011). Epithelial tissues have varying degrees of susceptibility to Kras(G12D)-initiated tumorigenesis in a mouse model. PLoS One 6, e16786. [PubMed: 21311774]

Ryan DP, Hong TS, and Bardeesy N (2014). Pancreatic Adenocarcinoma. New England Journal of Medicine 371, 1039–1049. [PubMed: 25207767]

Saponaro C, Gmyr V, Thevenet J, Moerman E, Delalleau N, Pasquetti G, Coddeville A, Quenon A, Daoudi M, Hubert T, et al. (2019). The GLP1R Agonist Liraglutide Reduces Hyperglucagonemia Induced by the SGLT2 Inhibitor Dapagliflozin via Somatostatin Release. Cell Rep 28, 1447–1454 e1444. [PubMed: 31390560]

Schauer DP, Feigelson HS, Koebnick C, Caan B, Weinmann S, Leonard AC, Powers JD, Yenumula PR, and Arterburn DE (2019). Bariatric Surgery and the Risk of Cancer in a Large Multisite Cohort. Ann Surg 269, 95–101. [PubMed: 28938270]

Siegel RL, Miller KD, and Jemal A (2020). Cancer statistics, 2020. CA Cancer J Clin 70, 7–30. [PubMed: 31912902]

Skowronski AA, Ravussin Y, Leibel RL, and LeDuc CA (2017). Energy homeostasis in leptin deficient Lepob/ob mice. PLoS One 12, e0189784. [PubMed: 29261744]

Smith JP, Cooper TK, McGovern CO, Gilius EL, Zhong Q, Liao J, Molinolo AA, Gutkind JS, and Matters GL (2014). Cholecystokinin Receptor Antagonist Halts Progression of Pancreatic Cancer Precursor Lesions and Fibrosis in Mice. Pancreas 43, 1050–1059. [PubMed: 25058882]

Smith JP, and Solomon TE (2014). Cholecystokinin and pancreatic cancer: the chicken or the egg? Am J Physiol Gastrointest Liver Physiol 306, G91–G101. [PubMed: 24177032]

Speakman JR (2019). Use of high-fat diets to study rodent obesity as a model of human obesity. Int J Obes (Lond).

Storz P (2017). Acinar cell plasticity and development of pancreatic ductal adenocarcinoma. Nat Rev Gastroenterol Hepatol 14, 296–304. [PubMed: 28270694]

TCGA Research Network (2017). Integrated Genomic Characterization of Pancreatic Ductal Adenocarcinoma. Cancer Cell 32, 185–203. [PubMed: 28810144]

Ulrich CM, Himbert C, Holowatyj AN, and Hursting SD (2018). Energy balance and gastrointestinal cancer: risk, interventions, outcomes and mechanisms. Nat Rev Gastroenterol Hepatol 15, 683–698. [PubMed: 30158569]

Usman M, and Volpi EV (2018). DNA damage in obesity: Initiator, promoter and predictor of cancer. Mutat Res 778, 23–37. [PubMed: 30454680]

van de Bunt M, Manning Fox JE, Dai X, Barrett A, Grey C, Li L, Bennett AJ, Johnson PR, Rajotte RV, Gaulton KJ, et al. (2015). Transcript Expression Data from Human Islets Links Regulatory Signals from Genome-Wide Association Studies for Type 2 Diabetes and Glycemic Traits to Their Downstream Effectors. PLoS Genet 11, e1005694. [PubMed: 26624892]

van Dijk D, Sharma R, Nainys J, Yim K, Kathail P, Carr AJ, Burdziak C, Moon KR, Chaffer CL, Pattabiraman D, et al. (2018). Recovering Gene Interactions from Single-Cell Data Using Data Diffusion. Cell 174, 716–729 e727. [PubMed: 29961576]

Wang K, Li M, and Hakonarson H (2010). ANNOVAR: functional annotation of genetic variants from high-throughput sequencing data. Nucleic Acids Res 38, e164. [PubMed: 20601685]

Wang Y, Nasiri AR, Damsky WE, Perry CJ, Zhang XM, Rabin-Court A, Pollak MN, Shulman GI, and Perry RJ (2018). Uncoupling Hepatic Oxidative Phosphorylation Reduces Tumor Growth in Two Murine Models of Colon Cancer. Cell Rep 24, 47–55. [PubMed: 29972790]

Weir GC (2020). Glucolipotoxicity, beta-Cells, and Diabetes: The Emperor Has No Clothes. Diabetes 69, 273–278. [PubMed: 31519699]

Williams JA, and Goldfine ID (1985). The insulin-pancreatic acinar axis. Diabetes 34, 980–986. [PubMed: 2412919]

Wolpin BM, Bao Y, Qian ZR, Wu C, Kraft P, Ogino S, Stampfer MJ, Sato K, Ma J, Buring JE, et al. (2013). Hyperglycemia, insulin resistance, impaired pancreatic beta-cell function, and risk of pancreatic cancer. J Natl Cancer Inst 105, 1027–1035. [PubMed: 23847240]

Wolpin BM, Michaud DS, Giovannucci EL, Schernhammer ES, Stampfer MJ, Manson JE, Cochrane BB, Rohan TE, Ma J, Pollak MN, et al. (2007). Circulating insulin-like growth factor binding protein-1 and the risk of pancreatic cancer. Cancer Res 67, 7923–7928. [PubMed: 17699799]

Xu M, Jung X, Hines OJ, Eibl G, and Chen Y (2018). Obesity and Pancreatic Cancer: Overview of Epidemiology and Potential Prevention by Weight Loss. Pancreas 47, 158–162. [PubMed: 29346216]

Ying W, Lee YS, Dong Y, Seidman JS, Yang M, Isaac R, Seo JB, Yang BH, Wollam J, Riopel M, et al. (2019). Expansion of Islet-Resident Macrophages Leads to Inflammation Affecting beta Cell Proliferation and Function in Obesity. Cell Metab 29, 457–474 e455. [PubMed: 30595478]

Yuan C, Bao Y, Wu C, Kraft P, Ogino S, Ng K, Qian ZR, Rubinson DA, Stampfer MJ, Giovannucci EL, et al. (2013). Prediagnostic body mass index and pancreatic cancer survival. J Clin Oncol 31, 4229–4234. [PubMed: 24145341]

Zaytouni T, Tsai PY, Hitchcock DS, DuBois CD, Freinkman E, Lin L, Morales-Oyarvide V, Lenehan PJ, Wolpin BM, Mino-Kenudson M, et al. (2017). Critical role for arginase 2 in obesity-associated pancreatic cancer. Nat Commun 8, 242. [PubMed: 28808255]

Zhang AMY, Magrill J, de Winter TJJ, Hu X, Skovso S, Schaeffer DF, Kopp JL, and Johnson JD (2019). Endogenous Hyperinsulinemia Contributes to Pancreatic Cancer Development. Cell Metab 30, 403–404. [PubMed: 31378465]

Zhang YP, Wan YD, Sun YL, Li J, and Zhu RT (2015). Aspirin might reduce the incidence of pancreatic cancer: A meta-analysis of observational studies. Sci Rep 5, 15460. [PubMed: 26486090]

Zyromski NJ, Mathur A, Pitt HA, Wade TE, Wang S, Nakshatri P, Swartz-Basile DA, and Nakshatri H (2009). Obesity potentiates the growth and dissemination of pancreatic cancer. Surgery 146, 258–263. [PubMed: 19628082]

HIGHLIGHTS

- Obesity accelerates oncogenic *Kras-driven* pancreatic ductal tumorigenesis in mice
- Genetic or dietary weight loss intercepts pancreatic cancer progression
- Obesity is associated with aberrant pancreatic islet cholecystokinin expression
- Islet cholecystokinin overexpression drives pancreatic ductal cancer development

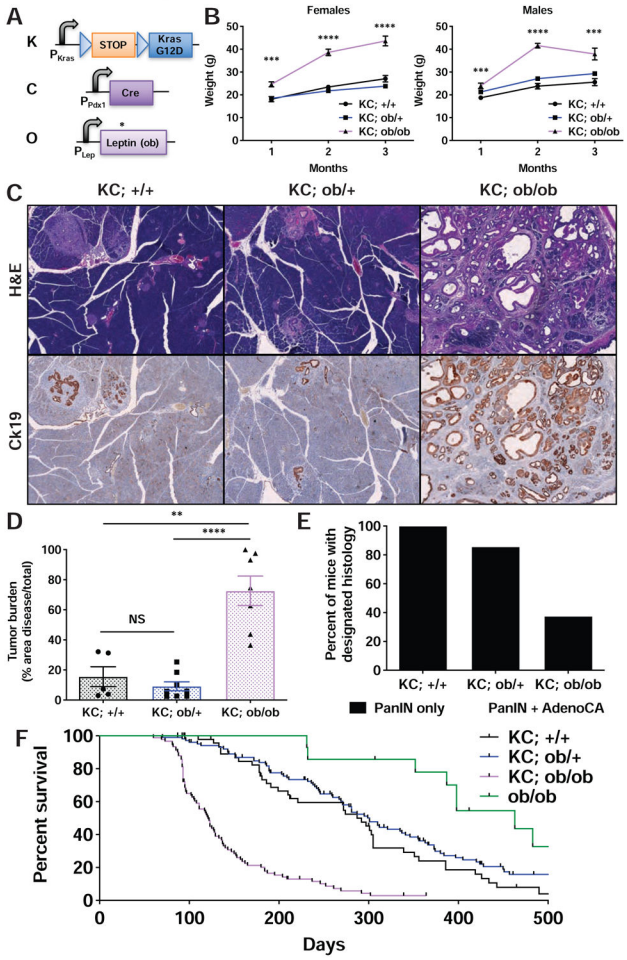

Figure 1. Accelerated PDAC progression in *KCO* mice.

A) Schematic of transgenic/knock-in alleles in leptin-deficient *KC* mice (*KC; ob/ob or KCO*). Black arrows denote promoters. *Kras* and *Lep* promoters are endogenous. Blue triangles denote LoxP sites. A STOP cassette prevents oncogenic *Kras* (*G12D*) expression prior to Cre-mediated recombination. * denotes point mutation in *ob* gene causing premature stop.

B) Body weight (mean +/− s.e.m.) of *KC* mice of varying *ob* genotype over time (n=22-46 mice/group). ***p<0.001, ****p<0.0001, *KC; ob/ob* compared to *KC;* +/+ mice, two-tailed student's t-test at each time point.

C) Representative histologic sections of pancreata from mice of designated genotypes at 3 months of age demonstrated differences in Ck19+ ductal tumor burden. Scale bar: 200 μm.

D) Tumor burden (mean +/− s.e.m.) in mice of designated genotypes at 3 months of age (n=5-8 mice/group). **p<0.01, ****p<0.0001, two-tailed student's t-test. NS = non-significant.

E) Percentage of mice in (D) harboring PanINs and/or adenocarcinoma.

F) Kaplan-Meier survival curves for mice of designated genotypes (n=14-106 mice/group). Log-rank test: p<0.0001 *KC;* +/+ vs. *KC; ob/ob*, p<0.0001 *KC; ob*/+ vs. *KC; ob/ob*, p>0.05 *KC;* +/+ vs. *KC; ob*/+ See also Figure S1.

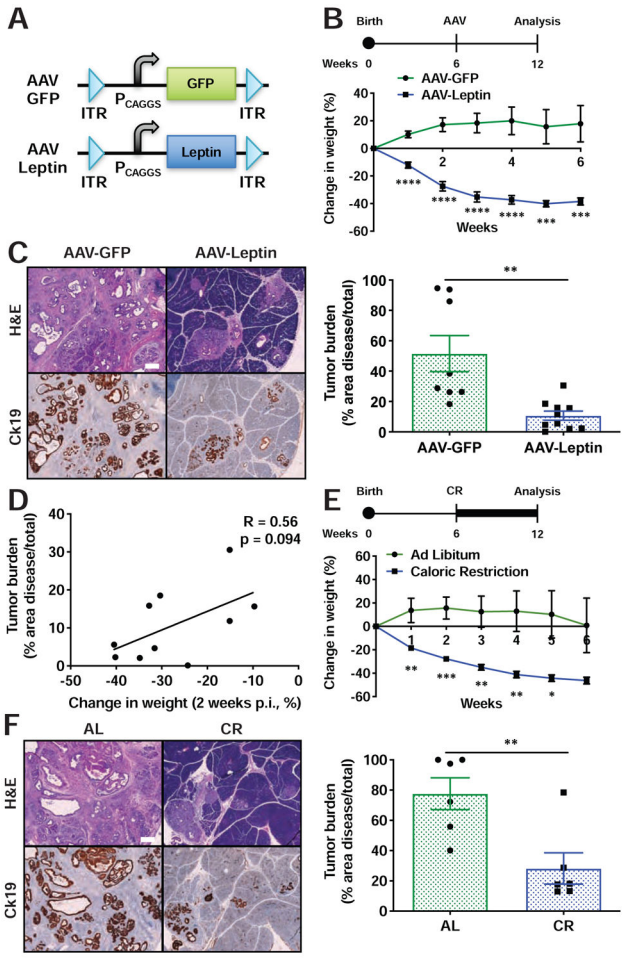

Figure 2. Weight loss intercepts early tumor progression in *KCO* mice.

A) Schematic of AAV vectors administered to *KCO* mice. ITR = internal tandem repeat for AAV2. CAGGS = CMV enhancer chicken beta-actin promoter. GFP = green fluorescent protein.

B) Schematic of AAV treatment for tumor interception experiment. AAV-GFP-treated mice served as controls. AAV was administered at 6 weeks of age prior to development of significant tumor burden. Mice were analyzed 6 weeks later. Percent change in body weight (mean +/− s.e.m., n=8-10 mice/group) following AAV administration is shown.

C) Representative histologic sections of pancreata of mice at endpoint in (B) demonstrated a reduction in Ck19+ ductal tumors with AAV-Leptin. Quantification of tumor burden (mean +/− s.e.m., n=8-10 mice/group) is shown.

D) Greater weight loss is associated with less tumor burden in mice treated with AAV-Leptin. Each point represents one mouse (n=10). Correlation coefficient (R) and p-value from simple linear regression are shown.

E) Schematic for caloric restriction (CR) experiment. Mice began CR at 6 weeks of age as in (B). Controls remained on ad libitum diet (AL). Percent change in body weight (mean +/− s.e.m., n=6 mice/group) following intervention is shown.

F) Representative histologic sections of pancreata of mice at endpoint in (E) demonstrated a reduction in Ck19+ ductal tumors with CR. Quantification of tumor burden (mean +/− s.e.m., n=6 mice/group) is shown.
$p<0.05$, $^{**}p<0.01$, $^{***}p<0.001$, $^{****}p<0.0001$, two-tailed student's t-test for all pairwise comparisons. Scale bars: 200 μm. See also Figure S2.

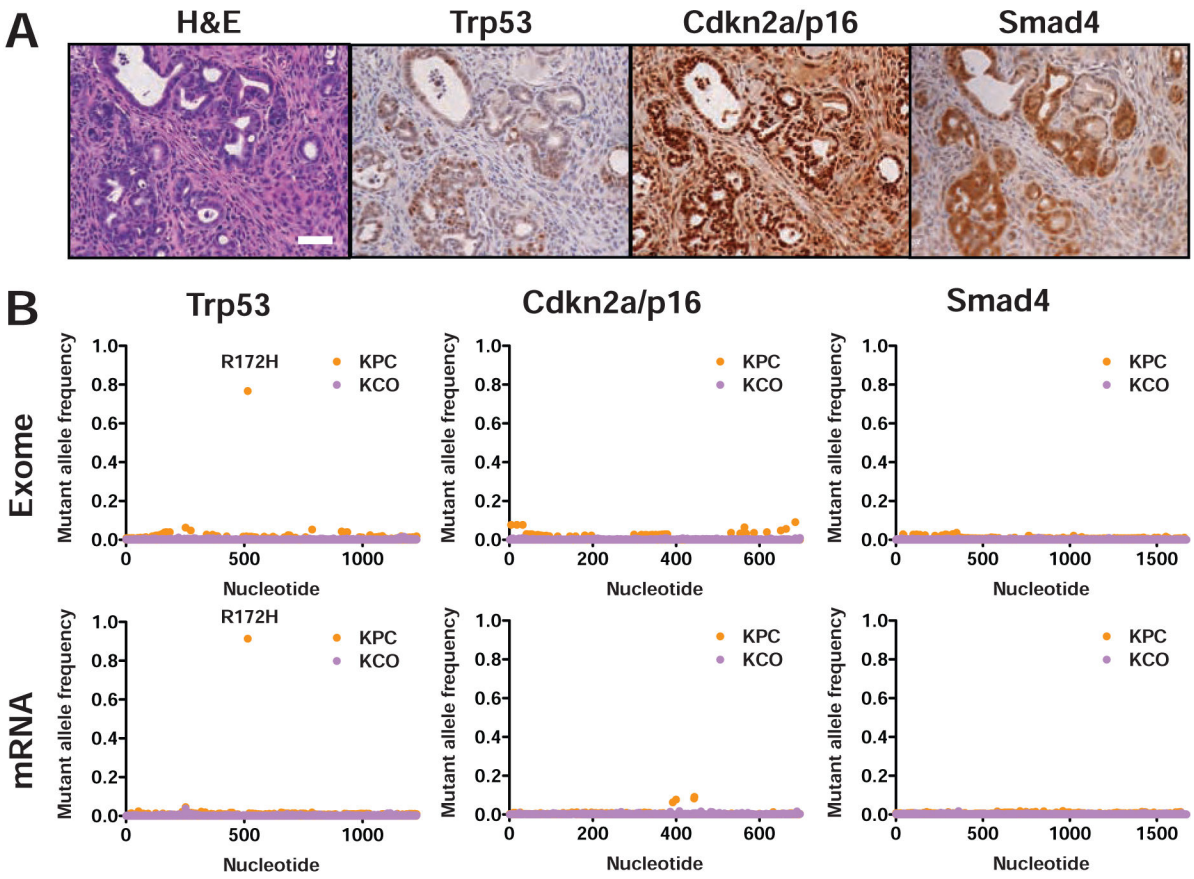

Figure 3. Obesity promotes tumor progression independent of new driver mutations.

A) Tumor suppressor proteins frequently mutated in human PDAC were retained in 8/8 (100%) *KCO* tumors analyzed by IHC. Scale bar: 50 μm.

B) Exome and mRNA sequencing did not reveal new single nucleotide variants in tumor suppressor genes in *KCO* tumors. Average mutant allele fraction identified for each base in the coding sequence is shown. A single *KPC* tumor sequenced in parallel shows the presence of the expected R172H codon change. See also Tables S1-S5.

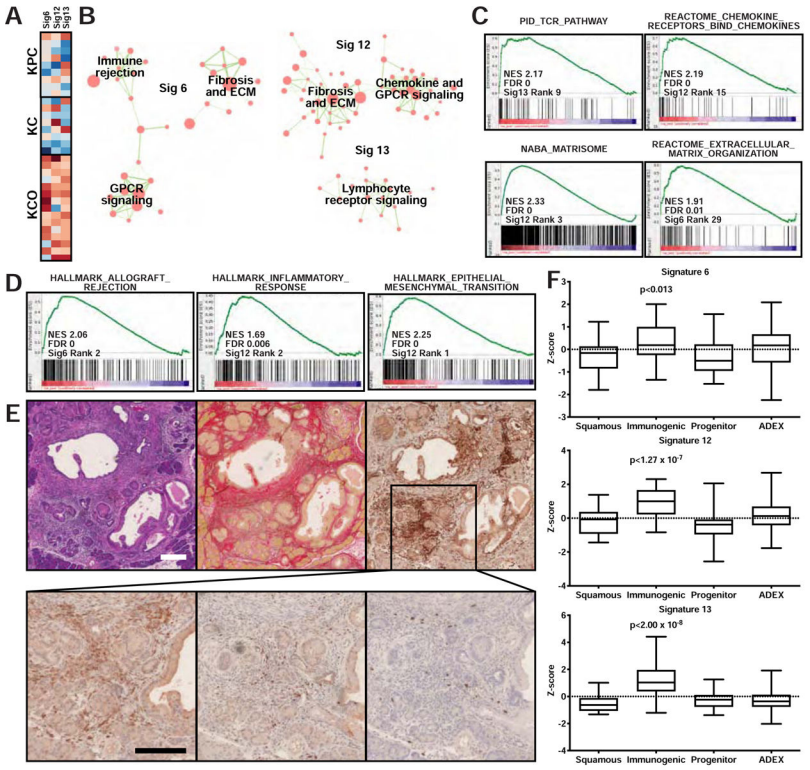

Figure 4. Enhanced inflammation and fibrosis in *KCO* tumors.

A) Heat map of row normalized Z-scores (of mixing weights from ICA decomposition) for gene expression signatures that separate tumors from obese (*KCO*) and non-obese (*KC* and *KPC*) models. See Methods for details. Rows represent individual tumors. Red corresponds to positive and blue to negative Z-scores.

B) Network representation of overlapping enriched GSEA/MSigDB curated (C2) gene sets associated with the *KCO* signatures in (A). Cellular processes associated with related gene sets are listed.

C) GSEA using the curated gene set collection (C2 in MSigDB) revealed an enrichment of genes involved in immune cell activation/signaling and extracellular matrix/fibrosis in *KCO* tumors See Table S6 for complete list.

D) GSEA showed an enrichment of inflammation and fibrosis gene sets (hallmark gene set collection (H in MSigDB)) with *KCO* tumors.

E) Histologic analyses revealed extensive fibrosis (Sirius red staining of collagen) and Cd45+ immune cell infiltration predominantly with F4/80+ macrophages and sparse presence of Cd3+ T and B220+ B cells. Scale bars: 100 μm

F) Box and whisker plots (boxes denote 25th-75th percentile, error bars denote min/max) of standardized signature scores for TCGA tumors corresponding to each molecular subtype (Bailey et al., 2016) are shown. See Methods for details. p-values confirmed significant enrichment of TCGA tumors highly-correlated to *KCO* signatures with the immunogenic subtype (hypergeometric test). See also Figure S3 and Table S6.

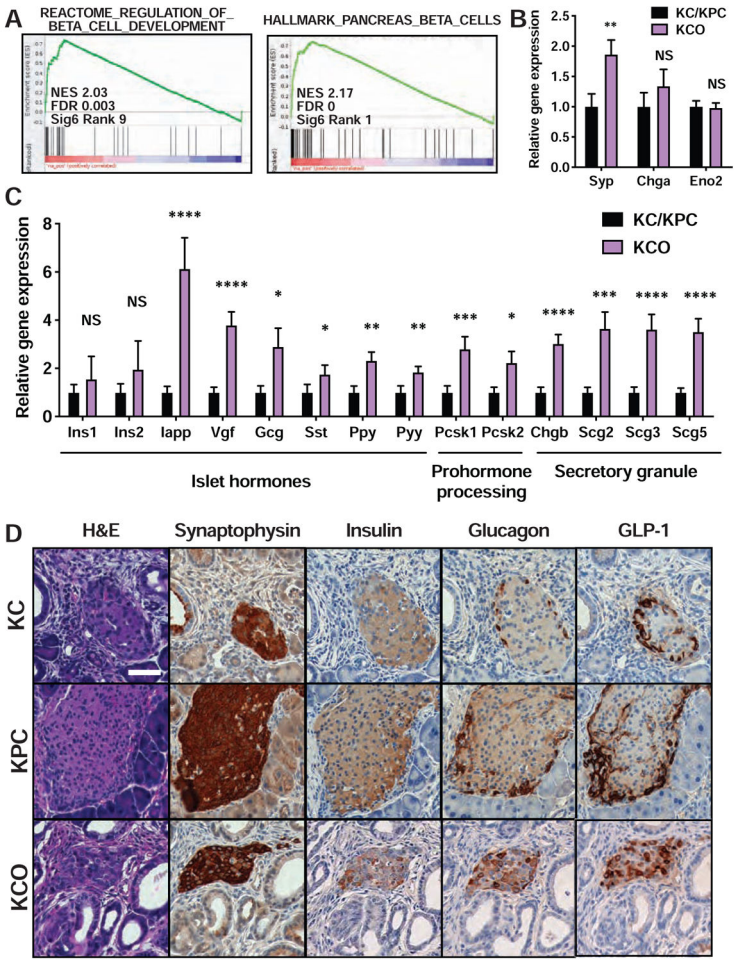

Figure 5. Pancreatic islet adaptation in *KCO* tumors.

A) GSEA using the curated (C2 in MSigDB) and hallmark (H in MSigDB) gene set collections revealed an association between *KCO* tumors and genes expressed in pancreatic beta cells. See Table S6 for complete list.

B) Relative gene expression (mean +/− s.e.m. normalized RNA-seq expression counts with non-obese *KC/KPC* tumors as baseline) for general neuroendocrine markers observed in pancreatic islet cells showed mild to no significant difference between *KCO* (n=15) and *KC/KPC* (n=17) tumors. **p<0.01, two-tailed Mann-Whitney test, comparing *KCO* to *KC/KPC*. NS = non-significant.

C) Relative gene expression (mean +/− s.e.m. normalized RNA-seq expression counts with *KC/KPC* tumors as baseline) of islet genes in tumors from *KCO* mice compared to non-obese models is shown. * p<0.05, **p<0.01, ***p<0.001, ****p<0.0001, two-tailed Mann-Whitney test, comparing *KCO* to *KC/KPC* expression for each gene.

D) IHC showed aberrant glucagon and GLP-1 expression throughout pancreatic islets in *KCO* mice compared to non-obese controls, consistent with upregulation of *Gcg* and *Pcsk1/Pcsk2* observed by RNA-seq in (C). Scale bar: 50 μm. See also Figure S4 and Table S6.

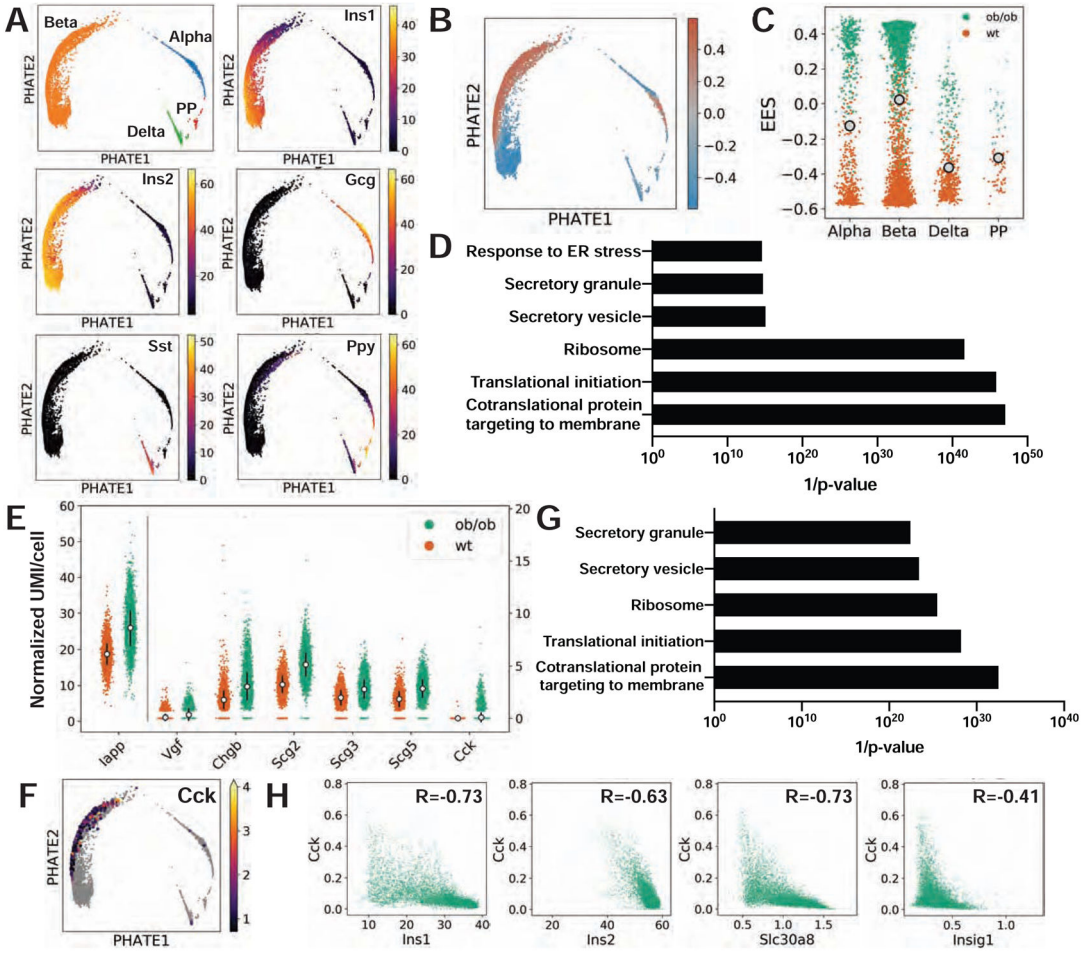

Figure 6. scRNA-seq identifies beta cell expression of *Cck* in obesity

A) PHATE visualization plots for single hormone-expressing islet clusters identified *Ins1/Ins2*+ beta cells, *Gcg*+ alpha cells, *Sst*+ delta cells, and *Ppy*+ PP cells amongst all sequenced cells.

B) PHATE plot colored by the Enhanced Experimental Signal (EES) values from MELD (Burkhardt et al., 2019) indicated the likelihood of observing each transcriptional profile in *ob/ob* (red) and wild-type (WT, blue).

C) The distribution of EES values in the clusters in (A) showed only moderate overlap in beta and alpha clusters between genotypes. Gray dots in each column mark the mean EES value in each cluster. Single cells color-coded by genotype showed a relative increase in beta cells in *ob/ob* islets (mean EES>0) and a proportional decrease in alpha, delta, and PP cells (mean EES<0).

D) Upregulated genes comparing *ob/ob* with WT beta cells showed significant overlap (hypergeometric test) with gene sets associated with protein translation and secretion.

E) Mean single cell expression counts (square-root transformed library size-normalized UMI/cell +/− s.d.) for beta cells showed upregulation of hormones and secretory granule genes in *ob/ob* islets. Each colored dot represents a single cell. Gray circles represent median expression.

F) PHATE visualization shows *Cck* expression exclusively in beta cells. *Cck* is expressed in *ob/ob*, but not WT, islets as shown in (E).

G) Upregulated genes comparing *Cck*+ versus *Cck*- *ob/ob* beta cells showed significant overlap (hypergeometric test) with gene sets associated with protein translation and secretion.

H) Gene-gene expression plots after MAGIC imputation (van Dijk et al., 2018) showed an inverse relationship between the expression of *Ins1, Ins2, Slc30a8,* and *Insig1* with *Cck* in *ob/ob* beta cells. Spearman correlation coefficients (R) are listed for each plot. See also Figures S5-S6 and Table S7.

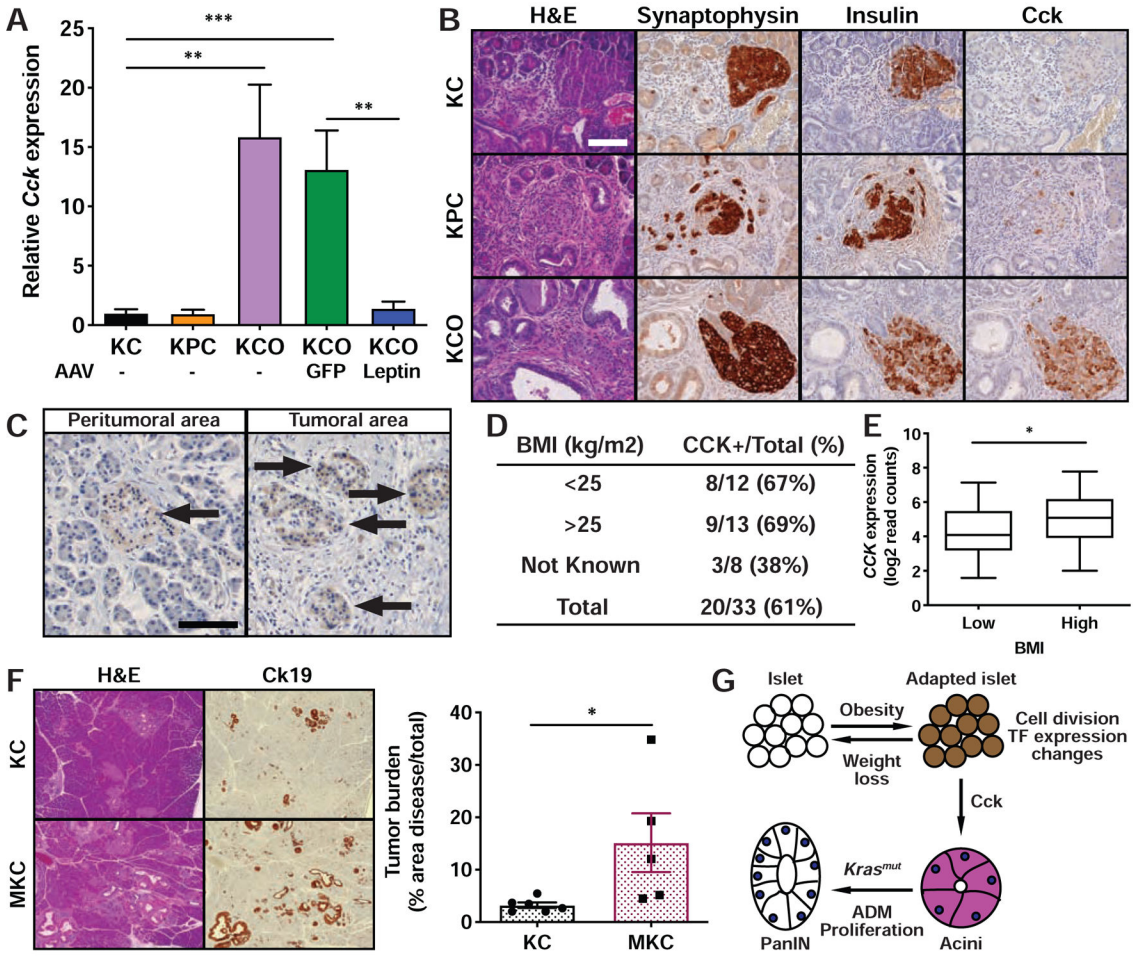

Figure 7. Islet-derived Cck promotes pancreatic ductal cancer development

A) Relative gene expression (mean +/− s.e.m. normalized RNA-seq expression counts with *KC* tumors as baseline) of *Cck* in obese (*KCO* and *KCO* mice treated with AAV-GFP) and non-obese models (*KC, KPC*, and *KCO* mice treated with AAV-Leptin) is shown (n=5-9 per group). **p<0.01, ***p<0.001, two-tailed Mann-Whitney test.

B) Cck was aberrantly overexpressed in pancreatic islets of *KCO* compared to *KC* and *KPC* mice. Scale bar: 100 μm.

C) CCK IHC on human PDAC tissues demonstrated expression specifically in islets (arrows). Scale bar: 100 μm.

D) The majority of human PDAC specimens displayed islet CCK expression by IHC at all BMI levels at diagnosis.

E) *CCK* expression in isolated pancreatic islets from human donors with high BMI (n=53, above median US BMI of 28.2 kg/m^2) was significantly (*p<0.05, two-tailed Mann-Whitney test) greater than from low BMI donors (n=55, below median). Box and whisker plots (boxes denote 25th-75th percentile, error bars denote min/max) are shown.

F) Representative histologic sections of pancreata demonstrated an increase in Ck19+ ductal tumorigenesis in *MKC (MIP-Cck; KC*) mice compared to *KC* mice. Quantification of tumor burden (mean +/− s.e.m., n=5-6 mice/group) at 3 months of age is shown. *p<0.05, two-tailed student's t-test. Scale bar: 200 μm.

G) Model for obesity-associated islet adaptations in PDAC development. Brown denotes Cck expression. ADM = acinar-to-ductal metaplasia. TF = transcription factor. See also Figures S3 and S7.

KEY RESOURCES TABLE

REAGENT or RESOURCE	SOURCE	IDENTIFIER
Antibodies		
Rat anti-B220	BD Biosciences	Cat# 550286; RRID:AB_393581
Rabbit anti-beta tubulin	Cell Signaling Technology	Cat# 2128; RRID:AB_823664
Rabbit anti-Cd3	Abcam	Cat# ab16669; RRID:AB_443425
Rabbit anti-Cd45 (LCA)	Abcam	Cat# ab10558; RRID:AB_442810
Rabbit anti-Cdkn2a	Abcam	Cat# ab54210; RRID:AB_881819
Rabbit anti-cholecystokinin	Immunostar	Cat# 20078; RRID:AB_572224
Rabbit anti-Ck19	Abcam	Cat# ab133496; RRID:AB_11155282
Mouse anti-Erk1/2	Cell Signaling Technology	Cat# 9107; RRID:AB_10695739
Rabbit anti-F4/80	Thermo Fisher Scientific	Cat# MA5-16363; RRID:AB_2537882
Rabbit anti-GFP	Cell Signaling Technology	Cat# 2956; RRID:AB_1196615
Mouse anti-Hsp90	BD Biosciences	Cat# 610418; RRID:AB_397798
Guinea pig anti-Insulin	Accurate Chemical	Cat# BMAT5014
Rabbit anti-Leptin (OB)	Santa Cruz Biotechnology	Cat# sc-842; RRID:AB_2136071
Rabbit anti-p53	Novacastra	Cat# NCL-p53-CM5p; RRID:AB_563933
Rabbit anti-pErk1/2 (T202/Y204)	Cell Signaling Technology	Cat# 4370; RRID:AB_2315112
Rabbit anti-pInsR/Igf1R (Y1162/Y1163)	Thermo Fisher Scientific	Cat# 44-804G; RRID:AB_2533762
Rabbit anti-pStat3 (Y705)	Cell Signaling Technology	Cat# 9145; RRID:AB_249100
Rabbit anti-Smad4	Abcam	Cat# ab40759; RRID:AB_777980
Mouse anti-Stat3	Cell Signaling Technology	Cat# 9139; RRID:AB_331757
Rabbit anti-Synaptophysin	Thermo Fisher Scientific	Cat# RB-1461; RRID:AB_60081
Anti-mouse IgG (H+L) (DyLight™ 680 Conjugate)	Cell Signaling Technology	Cat# 5470, RRID:AB_10696895
Anti-rabbit IgG (H+L) (DyLight™ 800 4X PEG Conjugate)	Cell Signaling Technology	Cat# 5151, RRID:AB_10697505
Peroxidase AffiniPure Goat Anti-Mouse IgG (H+L)	Jackson Immunoresearch	Cat# 115-035-146, RRID:AB_2307392
Peroxidase AffiniPure Goat Anti-Rabbit IgG (H+L)	Jackson Immunoresearch	Cat# 111-035-144, RRID:AB_2307391
Mach2 Rabbit HRP-Polymer	Biocare Medical	Cat# RHRP520
Mach2 Mouse HRP-Polymer	Biocare Medical	Cat# MHRP520
Rabbit anti-Ki67 (SP6)	Biocare Medical	Cat# CRM 325, RRID: AB_2721189
Rabbit anti-alpha-smooth muscle actin	Thermo Fisher Scientific	Cat# PA1-37024, RRID: AB_2223029
Peroxidase AffiniPure Donkey anti-guinea pig	Jackson Immunoresearch	Cat# 706-035-148, RRID: AB_2340447
Bacterial and Virus Strains		
One Shot Stbl3 chemically-competent E. coli	Thermo Fisher Scientific	Cat# C737303
AAV2/1CAGmLeptin	Custom-made AAV vector generated by the University of Iowa Viral Vector Core	N/A
AAV2/1CAGeGFP	University of Iowa Viral Vector Core	Cat# VVC-U of Iowa-640
Biological Samples		
Human pancreatitis biospecimens	University of Minnesota TP-IAT program	N/A
Human donor islets	Oxford Consortium for Islet Transplantation (OXCIT)	N/A

REAGENT or RESOURCE	SOURCE	IDENTIFIER
Human pancreatic cancer biospecimens	Dana-Farber Cancer Institute, University of Texas MD Anderson Cancer Center, University of Rochester, Stanford University	N/A
Chemicals, Peptides, and Recombinant Proteins		
Recombinant mouse leptin protein	R&D Systems	Cat# 498-OB
Aspirin USP	Spectrum Chemical	Cat# AS130
Metformin Hydrochloride, BP	Spectrum Chemical	Cat# M1566
Proglumide sodium salt	Sigma-Aldrich	Cat# M006
High-fat diet (60% kcal fat)	Research Diets, Inc.	Cat# D12492
Low-fat diet (10% kcal fat)	Research Diets, Inc.	Cat# 12240J
DNAse I	Worthington Biochemical	Cat# D2
Collagenase IV	Worthington Biochemical	Cat# CLS-4
Dispase	Worthington Biochemical	Cat# LS02100
TransIT LT1	Mirus Bio	Cat# MIR-2304
QuickExtract DNA extraction solution	Epicentre	Cat# QE0905
Puromycin dihydrochloride	Thermo Fisher Scientific	Cat# A1113803
Blasticidin S	Thermo Fisher Scientific	Cat# A1113903
Polybrene	EMD Millipore	Cat# TR-1003-G
Primestar HS	Takara	Cat# R040A
RIPA lysis and extraction buffer	Thermo Fisher Scientific	Cat# 89900
Halt protease/phosphatase inhibitor cocktail	Thermo Fisher Scientific	Cat# 78440
Cerulein	Sigma-Aldrich	Cat# C9026
Dapagliflozin	MedChemExpress	Cat# HY-10450
DMEM	Corning	Cat# 10-013-CV
DMEM	Sigma-Aldrich	Cat# D5030
Fetal Bovine Serum	Gibco/Thermo Fisher Scientific	Cat# 26140-079
Penicillin- Streptomycin	Gibco/Thermo Fisher Scientific	Cat# 15140-122
HEPES	Gibco/Thermo Fisher Scientific	Cat# 15630-080
L-glutamine	Gibco/Thermo Fisher Scientific	Cat# 25030-081
Q5 High-Fidelity 2X Master Mix	New England Biolabs	Cat# M0492S
Odyssey Blocking Buffer (PBS)	LI-COR Biosciences	Cat# 927-40000
Western Lightning Plus ECL	Perkin Elmer	Cat# NEL103001
L-arginine monohydrochloride	Sigma-Aldrich	Cat# A5131
GoTaq Green Master Mix	Promega	Cat# M7123
Critical Commercial Assays		
Mouse Leptin ELISA Kit	Crystal Chem	Cat# 90030, RRID:AB_2722664
Mouse CCK EIA Kit	RayBiotech	Cat# EIAM-CCK
Insulin RIA	Linco	Cat# RI-I3K
Mouse C-peptide ELISA Kit	Alpco Diagnostics	Cat# 80-CPTMS-E01, RRID: AB_2801468
CellTiter-Glo Luminescent Cell Viability Assay	Promega	Cat# G7570
High-Capacity cDNA Reverse Transcription Kit	Thermo Fisher Scientific	Cat# 4368814
Pierce BCA Protein Assay Kit	Thermo Fisher Scientific	Cat# 23227

REAGENT or RESOURCE	SOURCE	IDENTIFIER
Allprep DNA/RNA Mini Kit	Qiagen	Cat# 80204
Quant-iT™ PicoGreen™ dsDNA Assay Kit	Thermo Fisher Scientific	Cat# P7589
SureSelectXT Mouse All Exon Kit	Agilent	Cat# 5190-4642
Mouse High Range Insulin ELISA Kit	Alpco Diagnostics	Cat# 80-INSMSH-E01
MACS Dead Cell Removal Kit	Miltenyi Biotec	Cat# 130-090-101
Chromium Single Cell 3 ' Reagent Kit v3	10X Genomics	Cat# PN-1000092
Deposited Data		
Mouse pancreatic tumor RNA-seq data	Generated in this study and deposited in NCBI GEO	Acc# GSE131714
Mouse islet single cell RNA-seq data	Generated in this study and deposited in NCBI GEO	Acc# GSE137236
Mouse pancreatic tumor Exome-seq data	Generated in this study and deposited in NCBI SRA	Acc# PRJNA544740
Human pancreatic ductal adenocarcinoma (PAAD) RNA-seq data	The Cancer Genome Atlas (https://tcga-data.nci.nih.gov/tcga); TCGA. *Cancer Cell*, 2017.	N/A
Experimental Models: Cell Lines		
KPC-7307	Derived in this study from a C57/B6 *KC; p53$^{R172H/WT}$* mice	N/A
KPC-7310	Derived in this study from a C57/B6 *KC; p53$^{R172H/WT}$* mice	N/A
293T	ATCC	Cat# CRL-3216, RRID:CVCL_0063
Experimental Models: Organisms/Strains		
Mouse: *ob*: B6.Cg-Lep^{ob}/J	Jackson Laboratories	IMSR Cat# JAX:000632, RRID:IMSR_JAX:000632
Mouse: *db*: B6.BKS(D)-Lepr^{db}	Jackson Laboratories	IMSR Cat# JAX:000697, RRID:IMSR_JAX:000697
Mouse: *Pdx1-Cre*: B6.FVB-Tg(Pdx1-cre)6Tuv/J	Jackson Laboratories	IMSR Cat# JAX:014647, RRID:IMSR_JAX:014647
Mouse: *p53^{flox}*: B6.129P2- Trp53^{tm1Brn}/J	Jackson Laboratories	IMSR Cat# JAX:008462, RRID:IMSR_JAX:008462
Mouse: *MADM11-GT*: Igs2$^{tm1(ACTB-EGFP,-tdTomato)Luo}$/J	Jackson Laboratories	IMSR Cat# JAX:013749, RRID:IMSR_JAX:013749
Mouse: *MADM11-TG*: Igs2$^{tm2(ACTB-tdTomato,-EGFP)Luo}$/J	Jackson Laboratories	IMSR Cat# JAX:013751, RRID:IMSR_JAX:013751
Mouse: *MIP-CCK*: B6-Tg(Ins1- CCK)^{Davis}	Gift from D.B. Davis (University of Wisconsin)	N/A
Mouse: *Kras$^{LSL-G12D}$*: B6.129S4- *Kras^{tm4Tyj}*/J	Tyler Jacks lab (MIT)	IMSR Cat# JAX:008179, RRID:IMSR_JAX:008179
Mouse: *p53$^{KO/WT}$*:129- *Trp53^{tm1Tyj}*/J	Tyler Jacks lab (MIT)	IMSR Cat# JAX:002080, RRID:IMSR_JAX:002080
Mouse: *p53$^{R172H/WT}$*: 129S-Trp53^{tm2Tyj}/J	Tyler Jacks lab (MIT)	IMSR Cat# JAX:008652, RRID:IMSR_JAX:008652
Mouse: *Kras^{LA2}*:129S/Sv- Kras^{tm3Tyj}/J	Tyler Jacks lab (MIT)	IMSR Cat# JAX:008185, RRID:IMSR_JAX:008185
Mouse: *C57BL/6J*: C57/B6	Jackson Laboratories	IMSR Cat# JAX:000664, RRID:IMSR_JAX:000664
Oligonucleotides		
Leptin cDNA Reverse	Koch Institute Swanson Biotechnology Center	TCAGCATTCAGGGCTAACATCCAACT

REAGENT or RESOURCE	SOURCE	IDENTIFIER
mLepR sgRNA Forward	Keck Biotechnology Center at Yale	CACCGTGAAAGCCACCAGACCTCGA
mLepR sgRNA Reverse	Keck Biotechnology Center at Yale	AAACTCGAGGTCTGGTGGCTTTCAC
mLepR Target Site Forward	Keck Biotechnology Center at Yale	GGTTCTCAGTGCACGCATTT
mLepR Target Site Reverse	Keck Biotechnology Center at Yale	ACAACGATTTTCCTGGCATCT
Leptin cDNA Forward	Koch Institute Swanson Biotechnology Center	ATGTGCTGGAGACCCCTGT
Recombinant DNA		
lentiGuide-puro	Addgene	Cat# 52963
lentiCas9-blast	Addgene	Cat# 52962
pFBAAVCAGmcsBgHpa	University of Iowa Viral Vector Core	Cat# G0345
psPAX2	Addgene	Cat# 12259
pCMV-VSV-G	Addgene	Cat# 8454
Software and Algorithms		
ImageJ	NIH	N/A
QuPath v0.1.2	Github	N/A
Prism v8.0	Graphpad	N/A
Image Studio Lite	LI-COR	N/A
PHATE	https://github.com/KrishnaswamyLab/PHATE	N/A
MAGIC	https://github.com/KrishnaswamyLab/MAGIC	N/A
FASTX-toolkit	Greg Hannon lab (http://hannonlab.cshl.edu/fastx_toolkit)	N/A
Burrows-Wheeler Aligner v0.5.5	Source Forge	N/A
Picard toolkit v1.21	Github	N/A
GATK v.1.0.5538	Broad Institute	N/A
ANNOVAR	http://annovar.openbioinformatics.org/	N/A
RSEM v.1.2.12	Dewey lab/Github	N/A
Cytoscape v.3.3.0	Cytoscape Consortium	N/A
Cell Ranger	10X Genomics	N/A
SAS v9.4	SAS Institute, Inc.	N/A
MELD	https://github.com/KrishnaswamyLab/MELD	N/A
diffxpy	https://github.com/theislab/diffxpy/	N/A
R package JADE	https://www.rdocumentation.org/packages/JADE/versions/1.1-0	N/A